HHS Public Access

Author manuscript

Bioconjug Chem. Author manuscript; available in PMC 2019 December 19.

Published in final edited form as:

Bioconjug Chem. 2018 December 19; 29(12): 4090–4103. doi:10.1021/acs.bioconjchem.8b00699.

An Efficient Method for Labeling Single Domain Antibody Fragments with ^{18}F Using Tetrazine-*Trans*-Cyclooctene Ligation and a Renal Brush Border Enzyme-Cleavable Linker

Zhengyuan Zhou[a], **Nick Devoogdt**[b], **Michael R. Zalutsky**[a], and **Ganesan Vaidyanathan**[a,*]

[a]Department of Radiology, Duke University Medical Center, Durham, North Carolina, USA 27710

[b]In vivo Cellular and Molecular Imaging laboratory, Vrije Universiteit Brussel, (VUB), 1090, Brussels, Belgium

Abstract

Single domain antibody fragments (sdAbs) labeled with ^{18}F have shown promise for assessing the status of oncological targets such as the human epidermal growth factor receptor 2 (HER2) by positron emission tomography (PET). Earlier, we evaluated two residualizing prosthetic agents for ^{18}F-labeling of anti-HER2 sdAbs; however, these methods resulted in poor labeling yields and high uptake of ^{18}F activity in the kidneys. To potentially mitigate these limitations, we have now developed an ^{18}F labeling method that utilizes the *trans-cyclooctene* (TCO)-tetrazine (Tz)-based inverse-electron demand Diels-Alder reaction (IEDDAR) in tandem with a renal brush border enzyme-cleavable glycine-lysine (GK) linker in the prosthetic moiety. The HER2-targeted sdAb 2Rs15d was derivatized with TCO-GK-PEG$_4$-NHS or TCO-PEG$_4$-NHS, which lacks the cleavable linker. As an additional control, the non HER2-specific sdAb R3B23 was derivatized with TCO-GK-PEG$_4$-NHS. The resultant sdAb conjugates were labeled with ^{18}F by IEDDAR using [^{18}F]AlF-NOTA-PEG$_4$-methyltetrazine. As a positive control, the 2Rs15d sdAb was radioiodinated using the well-characterized residualizing prosthetic agent, *N*-succinimidyl 4-guanidinomethyl-3-[^{125}I]iodobenzoate ([^{125}I]SGMIB). Synthesis of [^{18}F]AlF-NOTA-Tz-TCO-GK-2Rs15d was achieved with an overall radiochemical yield (RCY) of 17.8 ± 1.5% (n=5) in 90 min, a significant improvement over prior methods (3–4% in 2–3 h). In vitro assays indicated that [^{18}F]AlF-NOTA-Tz-TCO-GK-2Rs15d bound with high affinity and immunoreactivity to HER2. In normal mice, when normalized to co-injected [^{125}I]SGMIB-2Rs15d, the kidney uptake of [^{18}F]AlF-NOTA-Tz-TCO-GK-2Rs15d was 15- and 28-fold lower (P<0.001) than that seen for the non-cleavable control ([^{18}F]AlF-NOTA-Tz-TCO-2Rs15d) at 1 h and 3 h, respectively. Uptake of [^{18}F]AlF-NOTA-Tz-TCO-GK-2Rs15d in HER2-expressing SKOV-3 ovarian carcinoma xenografts implanted in athymic mice was about 80% of that seen for co-injected [^{125}I]SGMIB-2Rs15d. On the other hand, kidney uptake was 5–6-fold lower, and as a result, tumor-to-kidney ratios were 4-fold higher for [^{18}F]AlF-NOTA-Tz-TCO-GK-2Rs15d than those for [^{125}I]SGMIB-2Rs15d. SKOV-3 xenografts were clearly delineated even at 1 h after administration of [^{18}F]AlF-NOTA-Tz-TCO-GK-2Rs15d by Micro-PET/CT imaging with even higher contrast observed thereafter. In conclusion, this strategy warrants further evaluation for labeling small proteins such as sdAbs

*Corresponding Author: Ganesan Vaidyanathan, Ph.D., 161C, Bryan Research Building, 311 Research Drive, Durham, North Carolina 27710, USA. Tel.: (919) 684-7811; ganesan.v@duke.edu.

because it offers the benefits of good radiochemical yields and enhanced tumor-to-normal tissue ratios, particularly in the kidney.

Graphical Abstract

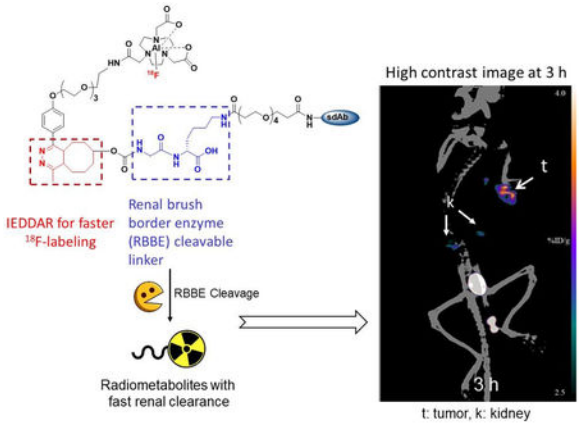

Keywords

HER2; Single domain antibody fragment (VHH, Nanobody); Fluorine-18; Inverse electron-demand Diels-Alder reaction; PET imaging; Brush border enzyme-cleavable linker

INTRODUCTION

Derived from Camelid heavy-chain-only antibodies, single-domain antibody fragments (sdAbs) have drawn tremendous attention as a potential platform for developing theranostic agents. Advantages of sdAbs for this purpose include the ability to readily develop molecules with high binding affinity even to sterically constrained molecular targets, high stability and low immunogenicity.[1] Consequently, sdAbs specific for various oncological targets have been developed and radiolabeled with an assortment of radionuclides.[2–9] The low molecular weight (<15 kDa) of sdAbs enables their rapid tumor localization and normal tissue clearance, which makes them an attractive and versatile vehicle for developing molecular targeted imaging agents for positron emission tomography (PET) when labeled with the short-lived positron emitters ^{18}F and ^{68}Ga. Indeed, sdAbs labeled with these two radionuclides currently are being explored for cancer detection and real time assessment of oncoprotein status.[10–13] These and other studies have confirmed that the relatively small size of these proteins facilitates tumor penetration and clearance of radioactivity from normal tissues; however, it also contributes to significant accumulation of activity in kidneys. While this may not be a significant issue for the detection of tumors in anatomical locations that are not in the proximity to the kidneys, the radiation dose received by the kidneys could be problematic, particularly in the majority of patients who might benefit from sequential PET studies to monitor the course of their disease.

High and persistent localization of activity from radiolabeled peptides and low molecular weight antibody fragments in the kidneys has been attributed to several factors.[14–16] These

include electrostatic interaction between the negatively charged proximal tubular cell surface and positively charged molecules and endocytosis mediated by receptors such as megalin and cubulin. Strategies to reduce renal accumulation of activity by countering these factors have included administration of basic amino acids and the plasma expander gelofusine,[17] increasing the negative charge of the labeled entity via chemical modification,[15] and insertion of cleavable linkers.[18–19] Incorporation of renal brush border enzyme (BBE)-cleavable linkers such as glycine-lysine (GK) or glycine-tyrosine dipeptide between the radiolabeled moiety and the targeting vector significantly reduced renal activity levels from radiolabeled antibody fragments without concomitant reduction in their tumor uptake.[20–21]

In previous studies, we developed two methods for labeling HER2-targeted sdAbs with ^{18}F using residualizing prosthetic moieties that provided excellent tumor localization but unacceptably high renal activity levels. In the first method, a residualizing prosthetic agent containing a *N*-succinimidyl ester, [^{18}F]RL-I was first synthesized by Cu(I)-catalyzed azide-alkyne cycloaddition (CuAAC; click reaction), and subsequently conjugated to two anti-HER2 sdAbs 5F7 and 2Rs15d.[22, 23] Even though excellent HER2-binding affinity and specific tumor targeting were achieved, the labeling method was convoluted and the overall radiochemical yield (RCY) for the synthesis of labeled sdAb was only 3 – 4%. To potentially overcome this, 2Rs15d was labeled by another approach ([^{18}F]RL-II) wherein the sdAb was first modified with a prosthetic agent containing a guanidine (residualizing) and an azide (for click reaction) moiety, and the thus derivatized sdAb was radiolabeled via strain-promoted alkyne-azide cycloaddition (SPAAC) with an ^{18}F-labeled reagent containing a cyclooctyne moiety.[11] The overall process was easier and the total time for labeling was lower compared with that for the labeling using [^{18}F]RL-I; however, no significant improvement in overall radiochemical yield was achieved, primarily due to very low yield for the SPAAC reaction. As noted above, unacceptably high levels of activity in the kidneys were observed for the ^{18}F-labeled sdAb conjugates prepared using both methods.

The aim of the current study was two-fold — 1) to develop a method for ^{18}F-labeling of sdAbs with higher radiochemical yields and shorter synthesis time, and 2) to minimize uptake of activity from the labeled sdAbs in the kidneys. Our approach utilized the tetrazine (Tz)/*trans*-cyclooctene (TCO) [4 + 2] inverse electron demand Diels-Alder cycloaddition reaction (IEDDAR)[24, 25] for ^{18}F-labeling[26–29] of the sdAb to address the first objective and a BBE-cleavable linker to address the second. The second order rate constant for tetrazine-*trans*-cyclooctene IEDDAR is several orders of magnitude higher than that for most bioorthogonal ligation reactions. For example, its rate constant (10^4-10^6 $M^{-1}s^{-1}$) is 10^4 to 10^9-fold higher than that for SPAAC (10^{-4} to 10^0 $M^{-1}s^{-1}$) that we utilized in the [^{18}F]RL-II method.[29,30] IEDDAR can be performed at room temperature in physiologically compatible buffers without the use of a catalyst and in a very short duration (minutes). In addition to utilizing the IEDDAR, we included the brush border enzyme-cleavable GK dipeptide linker[31] in the prosthetic moiety to potentially reduce kidney activity levels.

In this study, the HER2-specific 2Rs15d sdAb was first derivatized with a prosthetic group containing the TCO moiety, GK dipeptide, and PEG_4 chain. Labeling of derivatized 2Rs15d with ^{18}F was accomplished via IEDDAR with a reagent containing the [^{18}F]AlF-NOTA moiety, a PEG_3 chain and a Tz moiety (see Scheme 3). PEG chains were included to

potentially reduce kidney uptake further[14,32] and to provide flexibility for interaction of TCO/Tz moieties from the coupling partners and allow enzyme accessibility. This radiolabeled sdAb was evaluated in vitro using the HER2-expressing SKOV-3 human ovarian carcinoma cell line and in vivo using athymic mice bearing SKOV-3 human ovarian carcinoma xenografts. To assess whether the GK linker helped reduce renal uptake, a similar ^{18}F-labeled conjugate but without the GK linker also was synthesized and evaluated.

RESULTS AND DISCUSSION

HER2-targeted sdAbs labeled with various radionuclides are being explored for imaging and therapy of HER2-expressing cancers in both preclinical research and in a clinical trial.[8, 9, 11, 13, 33] Because of its widespread availability and short half-life, ^{18}F is an attractive option for PET imaging with sdAbs provided that ^{18}F-labeling of sdAbs targeting internalizing receptors can be achieved with good tumor uptake and tumor-to-background ratios. With that goal in mind, we developed two ^{18}F-labeling methods involving residualizing prosthetic agents — [^{18}F]RL-I and [^{18}F]RL-II.[11, 23] Although excellent tumor targeting was achieved with sdAbs labeled using these methods in HER2-expressing cells in vitro and human tumor xenografts in vivo, the labeling procedures were too involved and overall radiolabeling yields were too low to be suited for clinical translation. Moreover, renal uptake of activity from sdAbs labeled by these methods was unacceptably high (~80–140%ID/g).[11, 23] The work described herein was undertaken to address these problems.

In this study, we decided to introduce the ^{18}F via an [^{18}F]AlF-NOTA complex rather than a directly labeled tetrazine or TCO moiety. Only a few studies have been reported wherein a tetrazine-bearing agent was directly labeled, presumably due to the instability of the tetrazine moiety to basic ^{18}F-labeling conditions.[34,35] Parenthetically, in a different context, we recently have been able to achieve better radiolabeling yields for the synthesis of a tetrazine-containing reagent. Given the instability of tetrazines for ^{18}F-labeling conditions, ^{18}F-labeled TCO reagents have been synthesized and utilized for IEDDAR in a number of studies; however, this approach also is not without problems. Both in vivo defluorination and radiolytically induced cis-to-trans isomerization have been reported.[36, 37] Labeling proteins —both heat-resistant and heat-sensitive—with ^{18}F by employing Al^{18}F chemistry has been reported.[28, 38, 39] An additional motivation for us to use this method was the potential of this prosthetic agent to impart residualizing ability, which might be more helpful when used to label other sdAb that undergo more extensive internalization.

Compound **7** was synthesized starting with commercially available compounds **1** and **2** in five steps (Scheme 1). Coupling of **1** with **2** rendered **3** in 65% yield, and TFA-mediated removal of Boc group from **3** gave **4** in 91% yield. Reaction of **4** with commercially available TCO-NHS delivered **5** in 85% yield. Removal of the Fmoc group in **5** with piperidine gave **6** in 47% yield. Finally, **6** was coupled with NHS-PEG$_4$-NHS to obtain **7** in 24% yield. The tetrazine-NOTA conjugate **10** was synthesized in a single step by coupling the commercially available reagents methyltetrazine-PEG$_4$-amine (**8**) and NOTA-NHS (**9**) in 36% yield (Scheme 2). The unlabeled aluminum fluoride complex of **10** (**11**) was synthesized at a very small scale by treatment of **10** with AlF_3 in 73% yield for use as an

HPLC standard. The NMR and mass spectrometry data for all novel compounds (only LCMS for **11**) were consistent with their structures.

In the conjugation of 2Rs15d with the TCO-GK-PEG_4-NHS ester (**7**) (Scheme 3), MALDI-TOF mass spectrometry analysis indicated that 85% of the sdAb was modified with the prosthetic moiety (Figure S1), with approximately 85% and 15% of the modified sdAb having 1 and 2 prosthetic groups, respectively. In the conjugation of 2Rs15d with the commercially available TCO-PEG_4-NHS ester that did not contain the GK dipeptide linker, MALDI-TOF mass spectrometry analysis indicated that about 65% of the sdAb molecules were modified with one prosthetic group (Figure S2). With the negative control sdAb that does not bind HER2 (R3B23), the conjugation reaction resulted in ~75% of the sdAb derivatized with 1 or 2 TCO-GK-PEG_4 moieties (Figure S3). The conjugation efficiencies observed in this study were higher compared with those obtained previously with *N*-succinimidyl 3-azidomethyl-5-guanidinomethylbenzoate,[11] even though substantially lower amounts of prosthetic agent were used in the current study (~1.3 vs 30 molar equivalents). It is likely that the enhanced conjugation efficiency is due to the greater water solubility of the prosthetic agents employed herein.

The decay-corrected radiochemical yield for the synthesis of [^{18}F]AlF-NOTA-tetrazine was 46.3 ± 4.1% (n=8), which is on par with those reported for most similar compounds[28, 40, 41] although in one case, 70–95% radiochemical conversion has been reported.[38] Differences in reaction conditions such as the type of organic solvent and/or the ratio of organic solvent to water[28] as well as the substrate structure might have contributed to yield variability. The radiochemical yield for IEDDAR between the TCO-GK-PEG_4-derivatized 2Rs15d and [^{18}F]AlF-NOTA-tetrazine was 52.0 ± 1.8% (n=5). The radiochemical yields for the single-run syntheses of [^{18}F]AlF-NOTA-Tz-TCO-2Rs15d and [^{18}F]AlF-NOTA-Tz-TCO-R3B23 by IEDDAR with [^{18}F]AlF-NOTA-tetrazine were 43.0% and 34.8%, respectively. A range of radiochemical yields (~25–100%) has been reported for the ^{18}F-labeling of proteins containing a TCO moiety via IEDDAR with ^{18}F-labeled Tz analogues.[28, 38, 42] A possible reason for lower yields in some cases might be the presence of excess unreacted precursor (**10** in our study). As done by others, we did not attempt HPLC separation of [^{18}F]**11** from **10** because they both elute with similar retention times (11.5 min and 12 min for **11** and **10**, respectively) on reversed-phase HPLC and it would increase the overall synthesis time. However, the amount of **10** used for the synthesis of [^{18}F]**11** was adjusted to a 1:1 molar ratio to the sdAb. Other factors also might have decreased yields somewhat. Although the second-order rate constant for IEDDAR is significantly higher than that for CuAAC and SPAAC, the efficiency of IEDDAR might depend on the structure and size of the protein biomolecule as well as on the type and length of spacer between the biomolecule and the TCO prosthetic group. These factors can affect the accessibility of the TCO prosthetic group on the protein to the Tz moiety on the radiolabeled complementary molecule; due to hydrophobicity of TCO moieties, they are often buried within the protein.[43] For example, only 10% of the TCO moieties attached directly to a monoclonal antibody without a spacer were determined to be functional, whereas TCO moieties introduced via PEG linkers were fully functional.[44] The somewhat lower yield that we obtained for [^{18}F]AlF-NOTA-Tz-TCO-GK-2Rs15d may not be due to the lack of a spacer because there was a PEG_4 linker

between the sdAb and TCO. Despite the moderate yields obtained for IEDDAR, [^{18}F]AlF-NOTA-Tz-TCO-GK-2Rs15d was synthesized in an overall decay-corrected radiochemical yield (based on initial [^{18}F]fluoride activity) of 17.8 ± 1.5% (n = 5) in 60–70 min. This is a significant improvement compared with our earlier reported methods for ^{18}F-labeling of sdAbs — [^{18}F]RL-I[45] and [^{18}F]RL-II[23] — with more than five times higher radiochemical yield obtained in a considerably shorter time. In addition, the overall radiochemical yields we obtained in the current study were considerably higher than those reported for labeling sdAbs with [^{18}F]SFB. Blykers et al.[46] and Xavier et al.[47] reported overall radiochemical yields of 5–15% for the labeling of an anti-MMR 3.49 sdAb and 2Rs15d, respectively, with [^{18}F]SFB involving a 3-h total labeling time; yields for conjugation of [^{18}F]SFB to the sdAbs were 20–30%. We reported a conjugation yield of 37.8 ± 11.5% for labeling sdAb 5F7 with [^{18}F]SFB.[45] On the other hand, it should be noted that labeling yields of 35–53% in <35 min were obtained for labeling an anti-CRIg sdAb with ^{18}F using and [^{18}F]AlF^{2+} strategy that did not involve IEDDAR.[10] However, in this case, the protein was derivatized with a proprietary ligand, which was reacted directly with [^{18}F]AlF^{2+} at room temperature avoiding the somewhat lengthy procedure of labeling **10** and purification by solid-phase extraction utilized herein. At any rate, the fast reaction kinetics of both IEDDAR and the complexation of [^{18}F]AlF^{2+} with the NOTA macrocycle facilitated simplification of the labeling procedure. As noted above, we used solid-phase extraction to isolate [^{18}F]AlF-NOTA-tetrazine from any unreacted [^{18}F]fluoride, [^{18}F]AlF complex, and excess $AlCl_3$. Evaporation of acetonitrile from the eluate took about 30 min. Although it was attempted only once, avoiding this solid-phase extraction step did not affect the IEDDAR to a significant degree allowing considerable reduction in overall duration of labeling. This approach will be further explored in future studies. A comparison of parameters for labeling 2Rs15d with [^{18}F]RL-I, [^{18}F]RL-II, and the current method is summarized in Table 1. Although only once in each case was performed, the lower yields obtained for the synthesis of [^{18}F]AlF-NOTA-Tz-TCO-2Rs15d and [^{18}F]AlF-NOTA-Tz-TCO-GK-R3B23 might be due to lower levels of TCO modification (for the former) and/or the larger size of the sdAb (13.9 kDa versus 12.6 kDa) for the latter.

The molar activity of the [^{18}F]AlF-NOTA-Tz-TCO-GK-2Rs15d conjugate was 4.25 – 8.36 MBq/nmol starting from 0.37 – 0.93 GBq of [^{18}F]fluoride. SDS-PAGE revealed a single radioactive band, which is consistent with the molecular weight of 2Rs15d (Figure 1a). The radiochemical purity was further verified by SE-HPLC, which showed a single peak (>99%) corresponding to the size of an sdAb (Figure 1b). Saturation binding assay performed using HER2-expressing SKOV-3 ovarian carcinoma cells yielded a K_d value of 6.2 ± 1.1 nM (Figure 1c). The immunoreactive fraction (IRF) of [^{18}F]AlF-NOTA-Tz-TCO-GK-2Rs15d, determined by Lindmo assay, was 80.0 ± 5.9% (n=3; Figure 1d). These K_d and IRF values are comparable to those reported for 2Rs15d labeled using other methods[11, 23, 48] suggesting that ^{18}F-labeling of 2Rs15d using [^{18}F]AlF-NOTA-Tz-TCO-GK prosthetic agent did not compromise its binding to HER2.

The in vitro stability of the [^{18}F]AlF-NOTA-Tz-TCO-GK-2Rs15d conjugate was tested by incubation with mouse serum at 37°C. When analyzed by radio-SE-HPLC, negligible decomposition was seen, with more than 96% of the activity associated with the sdAb

throughout the 3-h study. In comparison, 98% and 92% radiochemical purity was reported for an affibody labeled using the [^{18}F]AlF-NOTA and [^{18}F]AlF-NODA prosthetic agents, respectively, after a 1-h incubation in mouse serum at 37°C.[38] As surmised by these authors, the low molecular weight ^{18}F-labeled compound(s) released from [^{18}F]AlF-NOTA-Tz-TCO-GK-2Rs15d most likely is the free [^{18}F]AlF complex. The stability observed for [^{18}F]AlF-NOTA-Tz-TCO-GK-2Rs15d should be sufficient for potential application as an imaging agent.

In the cell culture and in vivo experiments described below, [^{125}I]SGMIB-2Rs15d was used as a benchmark for comparison because this labeling approach has offered the best tumor targeting in preclinical studies,[8] and a clinical trial of the ^{131}I-labeled conjugate is currently underway in normal subjects and breast cancer patients (NCT02683083; *clinicaltirals.gov)*. The cellular uptake of [^{18}F]AlF-NOTA-Tz-TCO-GK-2Rs15d, as well as the ^{18}F-labeled analogous [^{18}F]AlF-NOTA-Tz-TCO-2Rs15d conjugate lacking the cleavable linker, were evaluated in HER2-expressing SKOV-3 ovarian carcinoma cells, each in tandem with [^{125}I]SGMIB-2Rs15d. As shown in Figure 2a and 2b, 6–8% of the [^{18}F]AlF-NOTA-Tz-TCO-GK-2Rs15d and [^{18}F]AlF-NOTA-Tz-TCO-2Rs15d added to the incubation media was specifically bound to cells over 1–4 h period. On the other hand, the specific uptake of co-incubated [^{125}I]SGMIB-2Rs15d was significantly higher at 17–24%, which was similar to that reported previously for this molecule.[11] Although there was some difference in the uptake of [^{18}F]AlF-NOTA-Tz-TCO-GK-2Rs15d and [^{18}F]AlF-NOTA-Tz-TCO-2Rs15d, the difference was not statistically significant when the values were normalized to those for the co-incubated [^{125}I]SGMIB-2Rs15d ($P > 0.05$), suggesting that the cleavable linker did not compromise binding or retention of activity in tumor cells. The about two-to-three-fold lower cell uptake of the ^{18}F-labeled constructs compared with [^{125}I]SGMIB-2Rs15d is not likely due to impaired binding to HER2 given their high immunoreactivity and HER2 binding affinity to HER2. A possible explanation is that [^{18}F]AlF-NOTA-containing prosthetic agents used herein are not residualizing like SGMIB; however, this may not be the main factor, given the modest degree of internalization of this anti-HER2 sdAb after cell binding.[11] Nonetheless, one report proposed that Al[^{18}F]$^{2+}$ chelated with NOTA is residualizing in nature,[49] while another suggested that Al[^{18}F]$^{2+}$ complexed with an analogous chelating moiety, RESCA, is non-residualizing.[10] Further studies are planned to investigate the reasons for the lower uptake of these ^{18}F-labeled sdAb conjugates on HER2-expressing cancer cells.

In order to investigate whether the inclusion of a brush border enzyme-cleavable linker in the prosthetic group could lower the activity levels of radiolabeled sdAbs in the kidneys, two paired-label biodistribution studies were performed in normal mice with [^{18}F]AlF-NOTA-Tz-TCO-GK-2Rs15d and [^{18}F]AlF-NOTA-Tz-TCO-2Rs15d, both administered in tandem with [^{125}I]SGMIB-2Rs15d. As shown in Figure 3a, the kidney uptake of activity from [^{18}F]AlF-NOTA-Tz-TCO-GK-2Rs15d at 1 h was about 5-fold lower than that for co-injected [^{125}I]SGMIB-2Rs15d. In contrast, the kidney uptake of [^{18}F]AlF-NOTA-Tz-TCO-2Rs15d was 3-fold higher than that seen for co-injected [^{125}I]SGMIB-2Rs15d (Figure 3b). To facilitate comparison of the two ^{18}F-labeled 2Rs15d conjugates, the kidney uptake values for the ^{18}F-labeled sdAbs were normalized to those obtained for the co-injected [^{125}I]SGMIB-2Rs15d sdAb in each study and the data are presented in Figure 3c. Expressed

as $^{18}F/^{125}I$ uptake ratios, these data show that the renal uptake of [^{18}F]AlF-NOTA-Tz-TCO-GK-2Rs15d was 15- and 28-fold lower than that for [^{18}F]AlF-NOTA-Tz-TCO-2Rs15d at 1 h and 3 h, respectively. These results are consistent with those observed when ~50 kDa antibody Fab fragments radioiodinated using prosthetic agents containing similar brush border enzyme-cleavable linkers.[20, 31] Thus, an important aspect of our study is that we have demonstrated that the brush border enzyme-cleavable linker strategy can be extended for use with a considerably smaller (<15 kDa) protein scaffold and to ^{18}F-labeled prosthetic agents.

Having demonstrated that incorporation of the cleavable linker resulted in a significant reduction in renal activity levels, we next evaluated the biodistribution of [^{18}F]AlF-NOTA-Tz-TCO-GK-2Rs15d in athymic mice with subcutaneous SKOV-3 xenografts to determine the effect of the linker on tumor-to-normal tissue ratios. Uptake of [^{18}F]AlF-NOTA-Tz-TCO-GK-2Rs15d in SKOV-3 xenografts was 3.46 ± 0.40% ID/g and 2.80 ± 0.31% ID/g at 1 h and 3 h, respectively (Table 2), values that were significantly lower ($P < 0.05$) than those seen for co-injected [^{125}I]SGMIB-2Rs15d (4.31 ± 0.52% ID/g at 1 h and 3.82 ± 0.65% ID/g at 3 h). In comparison, the tumor uptake observed earlier for [^{18}F]RL-II-2Rs15d in the same xenograft model (5.54 ± 0.77% ID/g at 1 h) was higher, and within error of that seen for co-administered [^{125}I]SGMIB-2Rs15d.[11] Furthermore, the tumor uptake obtained in the current study for [^{18}F]AlF-NOTA-Tz-TCO-GK-2Rs15d was lower than that reported (5.94 ± 1.17% ID/g at 1 h and 3.74 ± 0.52% ID/g at 3 h) in the same xenograft model for 2Rs15d labeled using the commonly used ^{18}F-labeling prosthetic agent *N*-succinimidyl 4-[^{18}F]fluorobenzoate ([^{18}F]SFB).[47] Combined with the in vitro uptake data observed in the SKOV-3 cell line (Figure 2), these results suggest that the [^{18}F]AlF-NOTA-Tz-TCO-GK prosthetic agent may not be highly residualizing. Another possibility is that the GK linker is susceptible to enzyme-mediated proteolysis in the SKOV-3 tumor environment. Although tumor uptake was not reported to be affected by the insertion of a brush border enzyme-cleavable linker in the case of a radiolabeled antibody Fab fragment,[31] differences in enzymatic accessibility between Fab and sdAb molecules, as well as proteolytic enzyme characteristics between cancer cell types may be factor(s).

Although the tumor uptake of [^{18}F]AlF-NOTA-Tz-TCO-GK-2Rs15d was lower than that seen for 2Rs15d labeled with ^{18}F using other methods, consistent with the study performed in normal mice, the kidney uptake levels observed for this radio-conjugate were 5–6-fold lower than those for co-administered [^{125}I]SGMIB-2Rs15d (see Table 2). As a result, tumor-to-kidney ratios were 4–5-fold higher for [^{18}F]AlF-NOTA-Tz-TCO-GK-2Rs15d than those for [^{125}I]SGMIB-2Rs15d (Figure 4). Importantly, the tumor-to-kidney ratio obtained at 1 h for [^{18}F]AlF-NOTA-Tz-TCO-GK-2Rs15d in this study (0.45) was higher than those reported for [^{18}F]RL-II-2Rs15d[11] (0.04) and [^{18}F]SFB-2Rs15d[47] (0.29). Likewise, the tumor-to-kidney ratio at 3 h (2.11) was substantially higher than those reported for [^{18}F]RL-II-2Rs15d (0.08) and [^{18}F]SFB-2Rs15d (0.98) at this time point.

With regard to the biodistribution of [^{18}F]AlF-NOTA-Tz-TCO-GK-2Rs15d in other normal tissues, the results obtained in athymic mice with SKOV-3 xenografts are also presented in Table 2; those obtained in BALB/c mice are given in Table S1. Biodistribution results for [^{18}F]AlF-NOTA-Tz-TCO-2Rs15d are summarized in Table S2. These molecules exhibited the typical behavior of sdAbs, with fast blood clearance observed for both [^{18}F]AlF-NOTA-

Tz-TCO-GK-2Rs15d and [^{125}I]SGMIB-2Rs15d, with <1% ID/g present in blood pool even at 1 h. With a few exceptions, the uptake in most tissues including liver, spleen, lung, muscle, and brain also was very low for both tracers. Generally, the uptake of ^{18}F was considerably lower than that seen for ^{125}I. On the other hand, uptake in the intestines was significantly higher for [^{18}F]AlF-NOTA-Tz-TCO-GK-2Rs15d than for co-administered [^{125}I]SGMIB-2Rs15d . For example, in the experiment performed in the SKOV-3 xenograft model, activity levels at 1 h in the small intestine were about four times higher for ^{18}F compared with ^{125}I (1.99 ± 0.46 %ID/g vs 0.53 ± 0.11% ID/g). Similar patterns were seen in the normal mice biodistribution studies performed with both [^{18}F]AIF-NOTA-Tz-TCO-GK-2Rs15d and [^{18}F]AlF-NOTA-Tz-TCO-2Rs15d (Table S1 and Table S2). Higher intestinal uptake of activity from proteins including sdAbs radiolabeled utilizing the TCO-Tz IEDDAR has been reported previously.[42, 50–52] Because intact radiolabeled sdAbs are expected to be predominantly eliminated via the kidneys, it is likely that the high activity levels observed in the intestines must be due to ^{18}F-labeled TCO-Tz-containing low molecular weight catabolites. Although both renal and fecal elimination pathways have been reported for ^{18}F-labeled tetrazine derivatives similar in structure to [^{18}F]**11**,[28, 53] unless modified with a hydrophilic moiety, the intrinsic hydrophobic character of tetrazine should favor hepatobiliary excretion.[53] Consistent with the above results, gall bladders were observed in the microPET images (see below) of tumor-bearing mice, potentially reflecting the uptake of hydrophobic catabolites in this organ. If the higher uptake in intestines and gall bladder is indeed due to ^{18}F-labeled Tz-TCO-containing catabolites, it may be possible to minimize this effect by inserting a brush border enzyme-cleavable or other similar linker between the [^{18}F]AIF-NOTA and Tz-TCO moieties. Finally, it is encouraging to note that the bone uptake after injection of [^{18}F]AlF-NOTA-Tz-TCO-GK-2Rs15d was minimal with only 0.29 ± 0.07% ID/g at 1 h and 0.10 ± 0.07% ID/g at 3 h; bone uptake of ^{18}F in normal mice was also quite low. These results indicate a high in vivo stability for [^{18}F]AlF-NOTA-Tz-TCO-GK-2Rs15d towards defluorination. Furthermore, these results are consistent with those obtained for peptides and affibody molecules labeled using the [^{18}F]AlF-NOTA moiety.[38, 49, 54]

Because the uptake of ^{18}F activity after administration of [^{18}F]AlF-NOTA-Tz-TCO-GK-2Rs15d in tissues other than kidneys was quite low (Table 2), most tumor-to-normal tissue ratios observed for [^{18}F]AlF-NOTA-Tz-TCO-GK-2Rs15d (Figure 4) were comparable or substantially higher than those reported for both [^{18}F]RL-II-2Rs15d and [^{18}F]SFB-2Rs15d.[11, 47] For example, the tumor-to-blood ratio for [^{18}F]AlF-NOTA-Tz-TCO-GK-2Rs15d was 14.3 ± 3.3 and 70.2 ± 43.2 at 1 h and 3 h, respectively. In comparison, the values reported for [^{18}F]SFB-2Rs15d at 1 h and 3 h were 13.1 ± 2.4 and 15.0 ± 3.2,[47] and a tumor-to-blood ratio of 6.2 ± 1.5 at 1 h was obtained for [^{18}F]RL-II-2Rs15d. Tumor-to-tissue ratios for [^{18}F]AlF-NOTA-Tz-TCO-GK-2Rs15d in muscle, liver and spleen at 1 h were 27.6 ± 3.8, 8.8 ± 1.1, and 25.6 ± 5.4, respectively, compared with values of 9.9 ± 3.5, 2.7 ± 1.1, and 7.6 ± 2.4 for [^{18}F]RL-II-2Rs15d.[11]

Maximum intensity projection images obtained in a representative athymic mouse with a subcutaneous SKOV-3 xenograft at 1, 2 and 3 h after administration of [^{18}F]AlF-NOTA-Tz-TCO-GK-2Rs15d are depicted in Figure 5a. Clear delineation of tumor can be seen even at 1

h, with minimal background activity observed except in kidneys and bladder. Consistent with the results of the necropsy biodistribution experiment, ^{18}F activity in kidneys cleared with time, while the gallbladder and intestines were visualized at 2 h. At 3 h, tumor exhibited the highest activity accumulation relative to other organs except for the bladder. The tumor uptake values (SUV/%ID/g-Max) obtained from the PET data were 1.0/4.7, 1.1/4.8, and 0.9/4.1 at 1 h, 2 h and 3 h, respectively. That the uptake in tumor was HER2-specific was demonstrated by the absence of activity accumulation in the tumor (%ID/g scale same in both Figure 5a and 5b) after administration of the nonspecific sdAb labeled using the same [^{18}F]AlF-NOTA-Tz-TCO-GK prosthetic agent ([^{18}F]AlF-NOTA-Tz-TCO-GK-R3B23; Figure 5b).

CONCLUSIONS

Herein we report a method for labeling sdAbs with ^{18}F utilizing the inverse electron demand Diels-Alder cycloaddition reaction in a considerably shorter duration and with significantly improved overall radiochemical yields compared with our previously described methods. The labeled sdAb demonstrated excellent affinity and immunoreactivity for HER2. By insertion of a brush border enzyme-cleavable linker between the ^{18}F-containing moiety and the sdAb facilitated reduction of renal activity levels more than 15-fold compared with [^{18}F]RL-II-2Rs15d and about 3-fold compared with that reported for [^{18}F]SFB-2Rs15d. Although tumor uptake of the labeled sdAb was only about 74–80% of that seen for the co-administered 2Rs15d radioiodinated using the prototypical residualizing prosthetic agent SGMIB, tumor-to-normal tissue ratios for the new [^{18}F]AlF-NOTA-Tz-TCO-GK-sdAb conjugate were higher not only than for the co-administered [^{125}I]SGMIB-sdAb but also those reported in the literature for 2Rs15d sdAb labeled with other prosthetic agents. To improve this labeling strategy, structural modifications are being investigated to minimize intestinal accumulation likely related to generation of lipophilic radiolabeled catabolites.

EXPERIMENTAL PROCEDURES

General.

All reagents were purchased from Sigma-Aldrich (St. Louis, MO) except where noted. Sodium [^{125}I]iodide [81.4 TBq (2200 Ci/mmoI] in 0.1 N NaOH was obtained from Perkin-Elmer Life and Analytical Sciences (Boston, MA). Synthesis of *N*-succinimidyl 4-guanidinomethyl-3-[^{125}I]iodobenzoate ([^{125}I]SGMIB) and its conjugation to sdAb was performed as reported before.[11] The glycine derivative, 2, 5-dioxopyrrolidin-1-yl (*tert*-butoxycarbonyl)glycinate (**1**), was obtained from Thermo Fisher (Waltham, MA) and the lysine derivative, N^6-(((9H-fluoren-9-yl)methoxy)carbonyl)-L-lysine from Bachem (Torrance, CA). (*E*)-cyclooct-4-en-1-yl (2,5-dioxopyrrolidin-1-yl) carbonate (TCO-NHS ester), 2,5-dioxopyrrolidin-1-yl (*E*)-1-(cyclooct-4-en-1-yloxy)-1-oxo-5,8,11,14-tetraoxa-2-azaheptadecan-17-oate (TCO-PEG$_4$-NHS ester), and 2-(2-(2-(2-(4-(6-methyl-1,2,4,5-tetrazin-3-yl)phenoxy)ethoxy)ethoxy)ethoxy)ethan-1-amine (methyltetrazine-PEG$_4$-amine) were obtained from Click Chemistry Tools (Scottsdale, Az). NOTA-NHS (2,2'-(7-(2-((2,5-dioxopyrrolidin-1-yl)oxy)-2-oxoethyl)-1,4,7-triazonane-1,4-diyl)diacetic acid) was obtained from CheMatech (Dijon, France). NHS-PEG$_4$-NHS (bis(2,5-dioxopyrrolidin-1-yl)

4,7,10,13-tetraoxahexadecanedioate) was purchased from BroadPharm (San Diego, CA). High performance liquid chromatography (HPLC) was performed using the following systems: 1) an Agilent 1260 Infinity System (Santa Clara, CA) equipped with a 1260 Infinity Multiple Wavelength Detector, and an Advion Expression^{L} Compact Mass Spectrometer (Ithaca, NY) in series; 2) an Agilent 1260 Infinity system equipped with a 1260 Infinity Multiple Wavelength Detector and a LabLogic Dual Scan-RAM (Tampa, FL) flow radioactivity detector/TLC scanner. The two systems were controlled by Advion Mass Express software and LabLogic Laura® software, respectively. For both radiolabeled and unlabeled compounds, HPLC was performed using an Agilent Poroshell EC-120 (9.4 mm I.D. × 250 mm, 2.7 μm) reversed-phase semi-preparative column. For both radiolabeled and unlabeled derivatized sdAbs, analytical and preparative size exclusion chromatography (SEC) HPLC was performed using a Tosoh Bioscience (Montgomeryville, PA) TSKgel SuperSW2000 (4.6 mm I.D. × 30 cm, 4 μm) column, which was eluted with PBS, pH 7 at a flow rate of 0.3 mL/min. Vivaspin® 500 Centrifugal Concentrators used for desalting the derivatized sdAbs, were purchased from Sigma-Aldrich (St. Louis, MO). Empore™ SPE C18 cartridges, used for concentrating HPLC samples, were purchased from 3M (Maplewood, MN). Disposable PD-10 desalting columns for gel filtration were purchased from GE Healthcare (Piscataway, NJ). Activity levels in various samples were assessed using automated gamma counters — either an LKB 1282 (Wallac, Finland) or a Perkin Elmer Wizard II (Shelton, CT). Proton and Carbon-13 NMR spectra of samples were obtained on a 400 MHz or a 500 MHz spectrometer (Varian/Agilent; Inova) and chemical shifts are reported in δ units using the residual solvent peaks as a reference. Mass spectra were recorded using an Advion Expression^{L} Compact Mass Spectrometer for electrospray ionization (ESI) LC/MS (see above) and/or an Agilent LCMS-TOF (ESI); the latter is a high-resolution mass spectrometer. For the determination of molecular weights of sdAbs, either the above Advion system (LCMS) or an Applied Biosystems DE-PRO Biospectrometry Workstation (for MALDI) were used.

Single domain antibodies, cells, culture conditions and the animal model.

Details of production, purification and characterization of the HER2-targeted 2Rs15d sdAb have been reported previously.[48] Cell culture reagents were purchased from Thermo Fisher Scientific (Waltham, MA) except where noted. SKOV-3 human ovarian carcinoma cells, obtained from the Duke University Cell Culture Facility, were grown in McCoy's 5A medium containing 10% fetal bovine serum and 1% Penicillin-Streptomycin. Cells were cultured at 37°C in a 5% CO_2 humidified incubator. All experiments involving animals were performed using a protocol approved by the Duke University IACUC. Subcutaneous SKOV-3 xenografts were established by inoculating 10-week old female athymic nude mice (obtained from an internal breeding colony maintained by the Duke University Division of Laboratory Animal Resources) with 5×10^6 SKOV-3 cells in 50% Matrigel (Corning Inc. NY) in the above medium (100 μL). The tumors were allowed to grow until they reached a volume of 350–500 mm^3 (6–8 weeks).

N^6(((9*H*-fluoren-9-yl)methoxy)carbonyl)-*N*^{6}((*tert*-butoxycarbonyl)glycyl)-l-lysine (3).

A mixture of 2,5-dioxopyrrolidin-1-yl (*tert*-butoxycarbonyl)glycinate (0.20 g, 0.74 mmol), *N*^{6}-(((9*H*-fluoren-9-yl)methoxy)carbonyl)-L-lysine (0.27 g, 0.74 mmol) and *N*,*N*-

diisopropylethylamine (0.28 g, 2.20 mmol) in DMF (5 mL) was stirred at 25°C for 3 h. The product from this mixture was isolated by semi-preparative HPLC using the Agilent Poroshell EC-120 (9.4 × 250 mm, 2.7 μm) reversed-phase semi-preparative column eluted at a flow rate of 3 mL/min with a gradient consisting of 0.1% TFA both in water (solvent A) and acetonitrile (solvent B); the proportion of B was linearly increased from 25% to 75% in 30 min. Under these conditions, the product eluted with a retention time (t_R) of 23 min. Pooled HPLC fractions containing the product were lyophilized to obtain 0.25 g (0.48 mmol, 64.9%) of compound **3** as white solid: ^{1}H-NMR (CD_3CN) δ_H = 1.37 (s, 9H), 1.65 (t, 2H), 1.79 (m, 2H), 3.03 (t, 2H), 3.65 (s, 1H), 4.17 (t, 1H), 7.29(t, 2H), 7.37(t, 2H), 7.60 (d, 2H), 7.78(d, 2H). ^{13}C-NMR (CD3CN) δ_C = 23.70, 28.95, 30.43, 32.16, 41.52, 48.52, 53.43, 67.28, 80.57, 121.34, 126.53, 128.46, 129.03, 142.48, 145.57, 157.90, 171.66, 174.34. LRMS (LCMS-ESI) *m*/*z*: 526.3 $(M+H)^+$. HRMS (ESI, *m*/*z*): calcd for $C_{28}H_{35}N_3O_7$ $(M+H)^+$: 526.2548; found: 526.2549 ± 0.0002 (n = 4).

N^6-(((9*H*-fluoren-9-yl)methoxy)carbonyl)-N^2-glycyl-l-lysine (4).

A 95:2.5:2.5 (v/v/v) mixture of TFA:water:tri-*iso*propyl silane (0.5 mL) was added to compound **3** (0.20 g; 0.38 mmol) and the mixture stirred at 25°C for 30 min. Solvents were evaporated to yield 186.5 mg (91.4%, based on trifluoroacetate salt) of compound **4** as colorless oil: ^{1}H-NMR (CD_3OH) δ_H = 1.10–1.40 (m, 6H), 2.94 (t, 2H), 3.59 (s, 2H), 4.02 (t, 1H), 4.17 (d, 2H), 4.28 (t, 1H), 7.15(t, 2H), 7.23(t, 2H), 7.47 (d, 2H), 7.62(d, 2H). ^{13}C-NMR (CD_3OH) δ_C = 13.23, 17.39, 18.81, 24.11, 28.99, 30.55, 32.41, 41.55, 53.88, 55.90, 67.70, 121.05, 128.25, 128.89, 142.70, 145.43, 159.05, 167.49, 175.14. LRMS (LCMS-ESI) *m*/*z*: 426.2 $(M+H)^+$. HRMS (ESI, *m*/*z*): calcd for $C_{23}H_{27}N_3O_5$ $(M+H)^+$: 426.2024; found: 426.2025 ± 0.0003 (n = 4).

N^6-(((9*H*-fluoren-9-yl)methoxy)carbonyl)-N^2-(((((*E*)-cyclooct-4-en-1-yl)oxy)carbonyl)glycyl)-l-lysine (5).

Compound **4** (20.0 mg, 47 μmol), TCO-NHS (12.5 mg, 47 μmol), and *N*,*N*-diisopropylethylamine (15.0 mg, 120 μmol) were taken in 300 μL DMF and the mixture stirred overnight at 25°C. The product was isolated by semi-preparative HPLC using the conditions described above for **3** to yield 23.1 mg (40 μmol, 85.3%) of compound **5** as a white solid: ^{1}H-NMR (CD_3CN) δ_H = 1.25–2.30 (m, 16H), 3.03 (d, 2H), 3.67 (s, 2H), 5.42 (m, 1H), 5.54 (m, 1H), 5.76 (s,2H), 6.93 (d, 1H), 7.38(t, 2H), 7.38(t, 2H), 7.62 (d, 2H), 7.79(d, 2H). ^{13}C-NMR (CD_3CN) δ_C = 23.70, 30.43, 32.16, 33.57, 35.19, 39.61, 41.51, 42.10, 48.55, 53.44, 67.28, 82.03, 121.36, 126.57, 128.49, 129.06, 134.04, 136.32, 142.52, 145.63, 157.88, 171.37, 174.27. LRMS (LCMS-ESI) *m*/*z*: 578.3 $(M+H)^+$. HRMS (ESI, *m*/*z*): calcd for $C_{32}H_{39}N_3O_7$ $(M+H)^+$: 578.2861; found: 578.2862 ± 0.0003 (n = 4).

((((*E*)-cyclooct-4-en-1-yl)oxy)carbonyl)glycyl-l-lysine (6).

Compound **5** (20.0 mg, 35 μmol), was dissolved in 300 μL of 20% piperidine in DMF and the mixture stirred for 30 min at 25°C. The crude mixture was purified by semi-preparative HPLC as above except a gradient with the proportion of solvent B linearly increased from 10% to 25% in 30 min was used. Solvents from the pooled HPLC fractions containing the product (t_R = 22 min) were lyophilized to obtain 5.8 mg (16.3 μmol, 47%) of compound **6** as

white solid: ^{1}H-NMR (CD_3CN: D_2O = 2:8) δ_H = 1.5–2.7 (m, 16H), 3.20, (t, 2H), 4.0 (s,2H), 5.75–5.95 (m, 3H). ^{13}C-NMR (CD_3CN: D_2O = 2:8) δ_c = 21.59, 26.01, 30.40, 31.82, 33.49, 37.61, 38.94, 40.21, 43.41, 54.21, 81.68, 132.94, 135.13, 157.52, 170.82, 177.72. LRMS (LCMS-ESI) *m*/*z*: 356.3 $(M+H)^+$. HRMS (ESI, *m*/*z*): calcd for $C_{17}H_{29}N_3O_5$ $(M+H)^+$: 356.2186; found: 356.2187 ± 0.0002 (n = 4).

(22*S*)-22-(2-(((((*E*)-cyclooct-4-en-1-yl)oxy)carbonyl)amino)acetamido)-1-((2,5-dioxopyrrolidin-1-yl)oxy)-1,16-dioxo-4,7,10,13-tetraoxa-17-azatricosan-23-oic acid (7, TCO-GK-PEG$_4$-NHS ester).

Compound **6** (5.8 mg, 16.3 μmol) and *N*,*N*-diisopropylethylamine (3.1 mg, 25 μmol) were taken in 200 μL DMF. This was added over 5 min to a stirred solution of NHS-PEG$_4$-NHS (7.9 mg, 16.3 μmol) in 100 μL DMF, and the mixture stirred at 25°C for 2 h. The mixture was subjected to semi-preparative HPLC as above but using a gradient wherein the proportion of solvent B was linearly increased from 15% to 50% in 30 min. Removal of solvents from the pooled HPLC fractions containing **7** (t_R = 20 min) by lyophilization delivered 2.7 mg (3.8 μmol, 23.5%) of a colorless oil: ^{1}H-NMR (DMF-d_7) δ_H =1.30–2.00 (m, 14H), 2.26–2.32 (m, 4H), 2.41 (t, 2H), 2.97 (t, 2H), 3.10–3.20 (m, 2H), 3.49 (s, 2H), 3.53–3.63 (m, 10H), 3.69 (t, 2H), 3.82 (t, 2H), 4.26–4.30 (m, 1H), 4.35–4.39 (m, 1H), 5.44–5.50 (m, 1H),5.58–5.64 (m, 1H), 7.01 (d,1H), 7.78 (t, 1H), 7.98(d, 1H). ^{13}C-NMR (DMF-d_7) δ_C = 24.02, 26.66, 31.93, 32.87, 37.61, 39.43, 39.42, 41.93, 44.78, 53.16, 66.67, 68.33, 71.06, 71.23, 71.34, 81.00, 133.67, 136.12, 157.56, 168.63, 170.57, 171.21, 171.26, 174.65. LRMS (LCMS-ESI) *m*/*z*: 729.4 $(M+H)^+$. HRMS (ESI, *m*/*z*) calcd for $C_{33}H_{52}N_4O_{14}$ $(M+H)^+$: 729.3553; found: 729.3557 ± 0.0006 (n = 4).

2,2'-(7-(14-(4-(6-Methyl-1,2,4,5-tetrazin-3-yl)phenoxy)-2-oxo-6,9,12-trioxa-3-azatetradecyl)-1,4,7-triazonane-1,4-diyl)diacetic acid (10, NOTA-Tz).

A mixture of methyltetrazine-PEG$_4$-amine (**8**; 9.0 mg, 25 μmol), NOTA-NHS (**9**; 10.0 mg, 25 μmol), and *N*,*N*-diisopropylethylamine (6.4 mg, 50 μmol) in DMF (300 μL) was stirred at 40°C overnight. The mixture was subjected to semi-preparative HPLC using conditions as described for **7** to obtain 5.9 mg (9.1 μmol, 36.4%) of **10** (t_R = 20.8 min) as a violet-colored solid: ^{1}H-NMR (D_2O) δ_H = 2.79 (s, 3H), 3.01 (s, 2H)3.07 (s, 3H), 3.20 (s, 3H), 3.35–3.45 (m, 3H), 3.55–3.80 (m, 10H), 3.95 (t, 2H), 4.30 (t, 2H), 7.15 (d, 2H), 8.25 (d, 2H). ^{13}C-NMR (D_2O) δ_C = 20.85, 39.56, 49.40, 51.79, 58.11, 60.32, 68.24, 70.27, 70.52, 70.57, 70.72, 116.33, 124.69, 130.59, 162.80, 164.32, 167.45, 174.57, 174.69. LRMS (LCMS-ESI) *m*/*z*: 649.6 $(M+H)^+$. HRMS (ESI, *m*/*z*) calcd for $C_{29}H_{44}N_8O_9$ $(M+H)^+$: 649.3304; found: 649.3307 ± 0.0004 (n = 4).

Synthesis of AlF-NOTA-Tz (11).

Solutions of **10** (1.9 mg, 3 μmol) in 100 μL acetonitrile and AlF_3 in 0.5 M sodium acetate buffer, pH 4 (80 mM, 100 μL) were mixed and heated at 100°C for 30 min. The mixture was cooled to room temperature and purified by semi-preparative HPLC as above but using a gradient with the proportion of solvent B linearly increased from 10% to 20% in 20 min. Solvents from the pooled HPLC fractions (t_R = 13.4 min) were removed by lyophilization to obtain 1.54 mg (2.2 μmol, 73.3%) of **11** as a violet-colored solid: LRMS (LCMS-ESI) *m*/*z*:

693.3 $(M+H)^+$. HRMS (ESI, *m*/*z*): calcd for $C_{29}H_{42}AlFN_8O_9$ $(M+H)^+$: 693.2952; found: 693.2955 ± 0.0004 (n = 4).

Synthesis of [^{18}F]AlF-NOTA-Tz ([^{18}F]11).

[^{18}F]AlF-NOTA-Tz was synthesized by adaptation of methods reported for similar compounds.[28, 38, 40] Fluorine-18 activity (PET-NET Solutions, Durham, NC) trapped on a QMA cartridge (ABX GMbH, Radeberg, Germany) was eluted with isotonic saline (3 × 100 μL). A solution of **10** (7 μg, 10.8 nmol) in 0.5 M sodium acetate, pH = 4 (10 μL) containing 2 mM $AlCl_3$, acetonitrile (40 μL) and 40 μL of saline containing the ^{18}F activity (0.37 – 0.93 GBq; 10 – 25 mCi) were mixed and then heated at 100°C for 15 min. The resultant solution containing [^{18}F]**11** was purified and concentrated by solid-phase extraction using an Empore™ SPE C18 cartridge eluted with acetonitrile (3 × 150 μL). Acetonitrile from the pooled fractions was evaporated to dryness.

Derivatization of sdAbs with TCO-GK-PEG$_4$-NHS (7) ester or TCO-PEG$_4$-NHS ester.

A solution of the sdAb (2Rs15d, 1.0 mg, 79 nmol) in 0.1 M borate buffer, pH 8.5 (300 μL) was added to **7** (70 μg, 96 nmol) or TCO-PEG$_4$-NHS ester (49 μg, 96 nmol) and the mixture stirred at 30°C for 2 h. The anti-paraprotein sdAb R3B23[55] (1.0 mg, 72 nmol), which has no affinity to HER2, was also derivatized with **7** (78 μg, 108 nmol) as a tool for determining nonspecific uptake. The derivatized and underivatized sdAbs were isolated from unreacted esters and other small molecules by SE-HPLC. For this, a TSKgel SuperSW2000 (4.6 mm I.D. × 30 cm, 4 μm) SEC column was eluted with PBS, pH 7.0, at a flow rate of 0.3 mL/min. The pooled HPLC fractions were desalted using a Vivaspin® 500 5K MWCO filter, and then lyophilized to dryness. The molecular weight of derivatized sdAbs was determined by MALDI-TOF Mass Spectrometry.

Labeling of derivatized sdAbs with ^{18}F via IEDDAR using [^{18}F]AlF-NOTA-Tz.

Solutions of sdAb (50 μL, 2 mg/mL) in PBS, pH 7.4 was added to a vial containing dried [^{18}F]**11** (0.10 – 0.16 GBq), and the mixture incubated at 20°C for 10 min. The labeled sdAbs were isolated by gel filtration over a PD-10 column eluted with PBS.

Determination of radiochemical purity of labeled sdAbs.

The radiochemical purity/integrity of the radiolabeled sdAbs was determined by two methods: 1) SE-HPLC was performed using the same conditions described above with ~5 μCi of the labeled sdAb. The t_R of labeled sdAbs and small molecules are 12.3 min and 17.6 min, respectively; 2) non-reducing SDS-PAGE and subsequent phosphor imaging using a Storage Phosphor System Cyclone Plus phosphor imager (Perkin-Elmer Life and Analytical Sciences, Downers Grove, IL) was used to assess the integrity of labeled sdAbs as previously described.[11]

In vitro stability of [^{18}F]AlF-NOTA-Tz-TCO-GK-2Rs15d.

The stability of [^{18}F]AlF-NOTA-Tz-TCO-GK-2Rs15d in vitro was assessed by incubating 1.85 MBq of purified sdAb in mouse serum (300 μL) at 37°C. At 1, 2, and 3 h, a 100 μL

aliquot of the incubation mixture was injected onto the SE-HPLC column. From the HPLC data, the percentage of total activity associated with intact sdAb was determined.

Determination of immunoreactivity and K_d.

The immunoreactive fraction of the labeled sdAb was determined using an adaptation of the Lindmo method.[56] Briefly, streptavidin-coated magnetic beads (PureBiotech, Middlesex, NJ) were conjugated with the extracellular domain of HER2, or human serum albumin as a negative control. Aliquots of the [^{18}F]AlF-NOTA-Tz-TCOGK-2Rs15d or [^{18}F]AlF-NOTA-Tz-TCO-2Rs15d (~5 ng) were incubated in duplicate with increasing concentrations of both positive (HER2) and negative (HSA) beads at room temperature for 40 min. The supernatants and the beads were separated using a magnetic separator, beads were washed with PBS, and the activity on the beads and combined supernatants was counted in a gamma counter. From these data, the percentage of specific binding (binding to HER2 - HSA-coated beads) was calculated at each bead concentration. The reciprocals of the percentage of specific binding were plotted against the reciprocals of bead concentration and the data were fit to a straight line by linear regression. The immunoreactive fraction was calculated as the reciprocal of the y-intercept value (infinite antigen concentration).

A saturation binding assay was performed on HER2-positive SKOV-3 ovarian carcinoma cells following a protocol described earlier.[11] Briefly, SKOV-3 cells were seeded in 24-well plates at a density of 8×10^4 cells/well/mL and incubated at 37°C overnight. Cells were washed and incubated at 4°C for 2 h with fresh cold medium containing increasing concentrations (0.1 to 300 nM; 0.6 mL total volume) of [^{18}F]AlF-NOTA-Tz-TCO-GK-2Rs15d or [^{18}F]AlF-NOTA-Tz-TCO-2Rs15d. The cells were washed twice with cold medium and lysed with 0.1% SDS and the activity in cell the lysates was counted using the automated gamma counter. Non-specific binding was determined in parallel assays performed by co-incubating cells with a 100-fold excess of unlabeled 2Rs15d. The data were fitted using GraphPad Prism software to determine K_d values.

Paired-label uptake of [^{18}F]AlF-NOTA-Tz-TCO-GK-2Rs15d vs. [^{125}I]SGMIB-2Rs15d and [^{18}F]AlF-NOTA-Tz-TCO-2Rs15d vs. [^{125}I]SGMIB-2Rs15d in SKOV-3 cells.

SKOV-3 cells (8×10^5 cells per well/3 mL) were seeded in 6-well plates and incubated overnight at 37°C. On the day of the experiment, the medium was replaced with 2 mL medium containing 5 nM each of [^{18}F]AlF-NOTA-Tz-TCO-GK-2Rs15d (or [^{18}F]AlF-NOTA-Tz-TCO-2Rs15d) and [^{125}I]SGMIB-2Rs15d, and the cells were incubated at 37°C. After 1 h, 2 h and 4 h, the cell culture supernatants were collected, and cells were lysed with 0.1% SDS. Activity in the cell culture supernatants and cell lysates was counted in an automated gamma counter. Cell-associated activity was calculated from these as the percentage of input dose. To determine nonspecific uptake, a parallel experiment was performed as above with the addition of a 100-fold molar excess of non-labeled 2Rs15d in the incubation medium. The experiment was performed in triplicates and the entire experiment was repeated thrice.

Biodistribution Studies.

Paired-label biodistribution of [^{18}F]AlF-NOTA-Tz-TCO-GK-2Rs15d (or [^{18}F]AlF-NOTA-Tz-TCO-2Rs15d) and [^{125}I]SGMIB-2Rs15d was performed in BALB/c normal and/or athymic mice with subcutaneous SKOV-3 ovarian carcinoma xenografts. Normal mice weighing 20–25 g received 259 kBq (7 μCi, 0.4–3.4 μg) of [^{18}F]AlF-NOTA-Tz-TCO-GK-2Rs15d (or [^{18}F]AlF-NOTA-Tz-TCO-2Rs15d) and 185 kBq (5 μCi, 0.6–1.0 μg) of [^{125}I]SGMIB-2Rs15d in 100 μL of PBS by intravenous bolus via the tail vein. Each SKOV-3 tumor bearing mouse weighing 20–25 g received 259 kBq (7 μCi, 0.5 μg) of [^{18}F]AlF-NOTA-Tz-TCO-GK-2Rs15d and 185 kBq (5 μCi, 0.7 μg) of [^{125}I]SGMIB-2Rs15d in 100 μL of PBS by intravenous bolus via the tail vein. At 1 h and 3 h post injection, blood and urine were collected from groups of 4–5 mice, which were then killed by isofluorane overdose. Tumor and normal tissues were harvested, blot-dried, weighed, and counted for activity along with injection standards. From these data, the percentage of injected dose (ID) per organ or per gram of tissue (%ID/g) were calculated. Statistical significance of differences in uptake between the two radionuclides was determined by the Student t-test using GraphPad QuickCalcs; a P value of <0.05 was considered to be significant.

Micro-PET/CT imaging.

Imaging of mice bearing subcutaneous SKOV-3 xenografts was performed on a Siemens Inveon micro-PET/CT system (Malvern, PA). Three mice were imaged at 1 h, 2 h and/or 3 h after administration of 1.0–2.7 MBq (27–73 μCi; 2–6 μg) [^{18}F]AlF-NOTA-Tz-TCO-GK-2Rs15d or 1.8–3.5 MBq (48–94 μCi; 5–10 μg) [^{18}F]AlF-NOTA-Tz-TCO-GK-R3B23. Mice were anesthetized using 2–3% isoflurane in oxygen and placed prone in the scanner gantry for a 5 min static PET acquisition followed by a 5 min CT scan. List mode PET data were histogram-processed, and the images reconstructed using a standard OSEM3D/MAP algorithm — 2 OSEM3D iterations, and 18 MAP iterations — with a cutoff (Nyquist) of 0.5. Images were corrected for attenuation (CT-based) and radioactive decay. Image analysis was performed using Inveon Research Workplace software.

Supplementary Material

Refer to Web version on PubMed Central for supplementary material.

ACKNOWLEDGEMENTS

This work was supported by National Institutes of Health Grants CA188177 and CA42324. The authors thank Elzbieta Krol (in vitro studies) and Xiao-Guang Zhao (in vivo studies) for their excellent technical assistance. The excellent support from Thomas Hawk, and Simone Degan for performance of the micro-PET/CT scans is greatly appreciated.

References

(1). Iezzi ME, Policastro L, Werbajh S, Podhajcer O, and Canziani GA (2018) Single-domain antibodies and the promise of modular targeting in cancer imaging and treatment. Front. Immunol 9, 273; doi: 10.3389/fimmu.2018.00273. [PubMed: 29520274]

(2). Wang H, Meng AM, Li SH, and Zhou XL (2017) A nanobody targeting carcinoembryonic antigen as a promising molecular probe for non-small cell lung cancer. Mol. Med. Rep 16, 625–30. [PubMed: 28586008]

(3). Verhelle A, Van Overbeke W, Peleman C, De Smet R, Zwaenepoel O, Lahoutte T, Van Dorpe J, Devoogdt N, and Gettemans J (2016) Non-iInvasive imaging of amyloid deposits in a mouse model of AGel using ^{99m}Tc-modified nanobodies and SPECT/CT. Mol. Imaging Biol 18, 887–97. [PubMed: 27130233]

(4). Bala G, Baudhuin H, Remory I, Gillis K, Debie P, Krasniqi A, Lahoutte T, Raes G, Devoogdt N, Cosyns B et al. (2018) Evaluation of [^{99m}Tc]radiolabeled macrophage mannose receptor-specific nanobodies for targeting of atherosclerotic lesions in mice. Mol. Imaging Biol. 20, 260–7. [PubMed: 28875290]

(5). Chatalic KL, Veldhoven-Zweistra J, Bolkestein M, Hoeben S, Koning GA, Boerman OC, de Jong M, and van Weerden WM (2015) A novel ^{111}In-labeled anti-prostate-specific membrane antigen nanobody for targeted SPECT/CT imaging of prostate cancer. J. Nucl. Med 56, 1094–9. [PubMed: 25977460]

(6). Krasniqi A, D'Huyvetter M, Xavier C, Van der Jeught K, Muyldermans S, Van Der Heyden J, Lahoutte T, Tavernier J, and Devoogdt N (2017) Theranostic radiolabeled anti-CD20 sdAb for targeted radionuclide therapy of Non-Hodgkin Lymphoma. Mol. Cancer Ther. 16, 2828–39. [PubMed: 29054987]

(7). Broos K, Keyaerts M, Lecocq Q, Renmans D, Nguyen T, Escors D, Liston A, Raes G, Breckpot K, and Devoogdt N (2017) Non-invasive assessment of murine PD L1 levels in syngeneic tumor models by nuclear imaging with nanobody tracers. Oncotarget 8, 41932–46. [PubMed: 28410210]

(8). D'Huyvetter M, De Vos J, Xavier C, Pruszynski M, Sterckx YGJ, Massa S, Raes G, Caveliers V, Zalutsky M, Lahoutte T et al. (2017) ^{131}I-labeled anti-HER2 camelid sdAb as a theranostic tool in cancer treatment. Clin. Cancer Res. 23, 6616–28. [PubMed: 28751451]

(9). Pruszynski M, D'Huyvetter M, Bruchertseifer F, Morgenstern A, and Lahoutte T (2018) Evaluation of an anti-HER2 nanobody labeled with ^{225}Ac for targeted alpha- particle therapy of cancer. Mol. Pharm 15, 1457–66. [PubMed: 29502411]

(10). Cleeren F, Lecina J, Ahamed M, Raes G, Devoogdt N, Caveliers V, McQuade P, Rubins DJ, Li W, Verbruggen A, Xavier C et al. (2017) Al^{18}F-Labeling of heat-sensitive biomolecules for positron emission tomography imaging. Theranostics 7, 2924–39. [PubMed: 28824726]

(11). Zhou Z, Chitneni SK, Devoogdt N, Zalutsky MR, and Vaidyanathan G (2018) Fluorine-18 labeling of an anti-HER2 VHH using a residualizing prosthetic group via a strain-promoted click reaction: Chemistry and preliminary evaluation. Bioorg. Med. Chem 26, 1939–49. [PubMed: 29534937]

(12). Massa S, Vikani N, Betti C, Ballet S, Vanderhaegen S, Steyaert J, Descamps B, Vanhove C, Bunschoten A, van Leeuwen FW et al. (2016) Sortase A-mediated site-specific labeling of camelid single-domain antibody-fragments: a versatile strategy for multiple molecular imaging modalities. Contrast Media Mol. Imaging 11, 328–39. [PubMed: 27147480]

(13). Keyaerts M, Xavier C, Heemskerk J, Devoogdt N, Everaert H, Ackaert C, Vanhoeij M, Duhoux FP, Gevaert T, Simon P et al. (2016) Phase I study of ^{68}Ga-HER2-nanobody for PET/CT assessment of HER2 expression in breast carcinoma. J. Nucl. Med 57, 27–33. [PubMed: 26449837]

(14). Akizawa H, Uehara T, and Arano Y (2008) Renal uptake and metabolism of radiopharmaceuticals derived from peptides and proteins. Adv. Drug. Deliv. Rev 60, 1319–28. [PubMed: 18508156]

(15). Bapst JP, and Eberle AN (2017) Receptor-mediated melanoma targeting with radiolabeled alpha-melanocyte-stimulating hormone: Relevance of the net charge of the ligand. Front. Endocrinol. (Lausanne) 8, 93; doi: 10.3389/fendo.2017.00093. [PubMed: 28491052]

(16). Vegt E, de Jong M, Wetzels JF, Masereeuw R, Melis M, Oyen WJ, Gotthardt M, and Boerman OC (2010) Renal toxicity of radiolabeled peptides and antibody fragments: mechanisms, impact on radionuclide therapy, and strategies for prevention. J. Nucl. Med 51, 1049–58. [PubMed: 20554737]

(17). Jin ZH, Furukawa T, Sogawa C, Claron M, Aung W, Tsuji AB, Wakizaka H, Zhang MR, Boturyn D, Dumy P et al. (2014) PET imaging and biodistribution analysis of the effects of succinylated gelatin combined with L-lysine on renal uptake and retention of ^{64}Cu-cyclam-RAFT-c(-RGDfK-)$_4$ in vivo. Eur. J. Pharm. Biopharm 86, 478–86. [PubMed: 24316338]

(18). Kukis DL, Novak-Hofer I, and DeNardo SJ (2001) Cleavable linkers to enhance selectivity of antibody-targeted therapy of cancer. Cancer. Biother. Radiopharm 16, 457–67. [PubMed: 11789023]

(19). Jodal A, Pape F, Becker-Pauly C, Maas O, Schibli R, and Behe M (2015) Evaluation of ^{111}In-labelled exendin-4 derivatives containing different meprin beta-specific cleavable linkers. PLoS One 10, e0123443. [PubMed: 25855967]

(20). Akizawa H, Imajima M, Hanaoka H, Uehara T, Satake S, and Arano Y (2013) Renal brush border enzyme-cleavable linkages for low renal radioactivity levels of radiolabeled antibody fragments. Bioconjug. Chem 24, 291–9. [PubMed: 23330714]

(21). Suzuki C, Uehara T, Kanazawa N, Wada S, Suzuki H, and Arano Y (2018) Preferential cleavage of a tripeptide linkage by enzymes on renal brush border membrane to reduce renal radioactivity levels of radiolabeled antibody fragments. J. Med. Chem 61, 5257–68. [PubMed: 29869881]

(22). Vaidyanathan G, McDougald D, Choi J, Koumarianou E, Weitzel D, Osada T, Lyerly HK, and Zalutsky MR (2016) Preclinical evaluation of ^{18}F-labeled anti-HER2 nanobody conjugates for imaging HER2 receptor expression by immuno-PET. J. Nucl. Med 57, 967–73. [PubMed: 26912425]

(23). Zhou Z, Vaidyanathan G, McDougald D, Kang CM, Balyasnikova I, Devoogdt N, Ta AN, McNaughton BR, and Zalutsky MR (2017) Fluorine-18 labeling of the HER2-targeting single-domain antibody 2Rs15d using a residualizing label and preclinical evaluation. Mol. Imaging Biol. 19, 867–77. [PubMed: 28409338]

(24). Oliveira BL, Guo Z, and Bernardes GJL (2017) Inverse electron demand Diels-Alder reactions in chemical biology. Chem. Soc. Rev 46, 4895–950. [PubMed: 28660957]

(25). Png ZM, Zeng H, Ye Q, and Xu J (2017) Inverse-electron-demand Diels-Alder reactions: Principles and applications. Chem. Asian J 12, 2142–59. [PubMed: 28497539]

(26). Reiner T and Zeglis BM (2014) The inverse electron demand Diels-Alder click reaction in radiochemistry. J. Labelled Comp. Radiopharm 57, 285–90. [PubMed: 24347429]

(27). Billaud EMF, Belderbos S, Cleeren F, Maes W, Van de Wouwer M, Koole M, Verbruggen A, Himmelreich U, Geukens N, and Bormans G (2017) Pretargeted PET imaging using a bioorthogonal ^{18}F-labeled trans-cyclooctene in an ovarian carcinoma model. Bioconjug. Chem 28, 2915–20. [PubMed: 29191024]

(28). Meyer JP, Houghton JL, Kozlowski P, Abdel-Atti D, Reiner T, Pillarsetty NV, Scholz WW, Zeglis BM, and Lewis JS (2016) ^{18}F-Based pretargeted PET imaging based on bioorthogonal Diels-Alder click chemistry. Bioconjug. Chem 27, 298–301. [PubMed: 26479967]

(29). Lang K, and Chin JW (2014) Bioorthogonal reactions for labeling proteins. ACS Chem. Biol 9, 16–20. [PubMed: 24432752]

(30). Ramil CP, Dong M, An P, Lewandowski TM, Yu Z, Miller LJ, and Lin Q (2017) Spirohexene-tetrazine ligation enables bioorthogonal labeling of class B G protein-coupled receptors in live cells. J. Am. Chem. Soc 139, 13376–86. [PubMed: 28876923]

(31). Arano Y, Fujioka Y, Akizawa H, Ono M, Uehara T, Wakisaka K, Nakayama M, Sakahara H, Konishi J, and Saji H (1999) Chemical design of radiolabeled antibody fragments for low renal radioactivity levels. Cancer Res. 59, 128–34. [PubMed: 9892197]

(32). Li L, Turatti F, Crow D, Bading JR, Anderson AL, Poku E, Yazaki PJ, Williams LE, Tamvakis D, Sanders P et al. (2010) Monodispersed DOTA-PEG-conjugated anti-TAG-72 diabody has low kidney uptake and high tumor-to-blood ratios resulting in improved ^{64}Cu PET. J. Nucl. Med 51, 1139–46. [PubMed: 20554731]

(33). D'Huyvetter M, Vincke C, Xavier C, Aerts A, Impens N, Baatout S, De Raeve H, Muyldermans S, Caveliers V, Devoogdt N et al. (2014) Targeted radionuclide therapy with a ^{177}Lu-labeled anti-HER2 nanobody. Theranostics 4, 708–20. [PubMed: 24883121]

(34). Li Z, Cai H, Hassink M, Blackman ML, Brown RC, Conti PS, and Fox JM (2010) Tetrazine-trans-cyclooctene ligation for the rapid construction of ^{18}F labeled probes. Chem. Commun. (Camb) 46, 8043–5. [PubMed: 20862423]

(35). Denk C, Svatunek D, Filip T, Wanek T, Lumpi D, Frohlich J, Kuntner C, and Mikula H (2014) Development of a ^{18}F-labeled tetrazine with favorable pharmacokinetics for bioorthogonal PET imaging. Angew. Chem. Int. Ed. Engl 53, 9655–9. [PubMed: 24989029]

(36). Collins J, Waldmann CM, Drake C, Slavik R, Ha NS, Sergeev M, Lazari M, Shen B, Chin FT, Moore M, et al. (2017) Production of diverse PET probes with limited resources: 24 ^{18}F-labeled compounds prepared with a single radiosynthesizer. Proc. Natl. Acad. Sci. U S A 114, 11309–14. [PubMed: 29073049]

(37). Wyffels L, Thomae D, Waldron AM, Fissers J, Dedeurwaerdere S, Van der Veken P, Joossens J, Stroobants S, Augustyns K, and Staelens S (2014) In vivo evaluation of ^{18}F-labeled TCO for pre-targeted PET imaging in the brain. Nucl. Med. Biol 41, 513–23. [PubMed: 24768149]

(38). Da Pieve C, Allott L, Martins CD, Vardon A, Ciobota DM, Kramer-Marek G, and Smith G (2016) Efficient [^{18}F]AlF Radiolabeling of ZHER3:8698 affibody molecule for imaging of HER3 positive tumors. Bioconjug. Chem 27, 1839–49. [PubMed: 27357023]

(39). Cleeren F, Lecina J, Bridoux J, Devoogdt N, Tshibangu T, Xavier C, and Bormans G (2018) Direct fluorine-18 labeling of heat-sensitive biomolecules for positron emission tomography imaging using the Al^{18}F-RESCA method. Nat. Protoc 13, 2330–47. [PubMed: 30250289]

(40). Shi X, Gao K, Huang H, and Gao R (2018) Pretargeted immuno-PET based on bioorthogonal chemistry for imaging EGFR positive colorectal cancer. Bioconjug. Chem 29, 250–54. [PubMed: 29338219]

(41). Meyer JP, Kozlowski P, Jackson J, Cunanan KM, Adumeau P, Dilling TR, Zeglis BM, and Lewis JS (2017) Exploring structural parameters for pretargeting radioligand optimization. J. Med. Chem 60, 8201–17. [PubMed: 28857566]

(42). Rashidian M, Keliher E, Dougan M, Juras PK, Cavallari M, Wojtkiewicz GR, Jacobsen J, Edens JG, Tas JM, Victora G et al. (2015) The use of ^{18}F-2-fluorodeoxyglucose (FDG) to label antibody fragments for immuno-PET of pancreatic cancer. ACS Cent. Sci 1, 142–47. [PubMed: 26955657]

(43). Maggi A, Ruivo E, Fissers J, Vangestel C, Chatterjee S, Joossens J, Sobott F, Staelens S, Stroobants S, Van Der Veken P et al. (2016) Development of a novel antibody-tetrazine conjugate for bioorthogonal pretargeting. Org. Biomol. Chem 14, 7544–51. [PubMed: 27431745]

(44). Rahim MK, Kota R, and Haun JB (2015) Enhancing reactivity for bioorthogonal pretargeting by unmasking antibody-conjugated trans-cyclooctenes. Bioconjug. Chem 26, 352–60. [PubMed: 25584926]

(45). Vaidyanathan G, McDougald D, Choi J, Pruszynski M, Koumarianou E, Zhou Z, and Zalutsky MR (2016) *N*-Succinimidyl 3-((4-(4-[^{18}F]fluorobutyl)-1H-1,2,3-triazol-1-yl)methyl)-5-(guanidinomethyl)ben zoate ([18F]SFBTMGMB): a residualizing label for 18F-labeling of internalizing biomolecules. Org. Biomol. Chem 14, 1261–71. [PubMed: 26645790]

(46). Blykers A, Schoonooghe S, Xavier C, D'Hoe K, Laoui D, D'Huyvetter M, Vaneycken I, Cleeren F, Bormans G, Heemskerk J et al. V. (2015) PET imaging of macrophage mannose receptor-expressing macrophages in tumor stroma using ^{18}F-radiolabeled camelid single-domain antibody fragments. J. Nucl. Med 56, 12–1271.

(47). Xavier C, Blykers A, Vaneycken I, D'Huyvetter M, Heemskerk J, Lahoutte T, Devoogdt N, and Caveliers V (2016) ^{18}F-nanobody for PET imaging of HER2 overexpressing tumors. Nucl. Med. Biol 43, 247–52. [PubMed: 27067045]

(48). Xavier C, Vaneycken I, D'Huyvetter M, Heemskerk J, Keyaerts M, Vincke C, Devoogdt N, Muyldermans S, Lahoutte T, and Caveliers V (2013) Synthesis, preclinical validation, dosimetry, and toxicity of ^{68}Ga-NOTA-anti-HER2 nanobodies for iPET imaging of HER2 receptor expression in cancer. J. Nucl. Med 54, 776–84. [PubMed: 23487015]

(49). Schoffelen R, Sharkey RM, Goldenberg DM, Franssen G, McBride WJ, Rossi EA, Chang CH, Laverman P, Disselhorst JA, Eek A et al. (2010) Pretargeted immuno-positron emission tomography imaging of carcinoembryonic antigen-expressing tumors with a bispecific antibody and a ^{68}Ga- and ^{18}F-labeled hapten peptide in mice with human tumor xenografts. Mol. Cancer Ther. 9, 1019–27. [PubMed: 20354120]

(50). Albu SA, Al-Karmi SA, Vito A, Dzandzi JP, Zlitni A, Beckford-Vera D, Blacker M, Janzen N, Patel RM, Capretta A et al. (2016) ^{125}I-Tetrazines and inverse-electron-demand Diels-Alder chemistry: A convenient radioiodination strategy for biomolecule labeling, screening, and biodistribution studies. Bioconjug. Chem 27, 207–16. [PubMed: 26699913]

(51). Yazdani A, Janzen N, Czorny S, Ungard RG, Miladinovic T, Singh G, and Valliant JF (2017) Preparation of tetrazine-containing [2 + 1] complexes of ^{99m}Tc and in vivo targeting using

bioorthogonal inverse electron demand Diels-Alder chemistry. Dalton Trans. 46, 14691–99. [PubMed: 28640297]

(52). Rashidian M, Wang L, Edens JG, Jacobsen JT, Hossain I, Wang Q, Victora GD, Vasdev N, Ploegh H, and Liang SH (2016) Enzyme-mediated modification of single-domain antibodies for imaging modalities with different characteristics. Angew. Chem. Int. Ed. Engl 55, 528–33. [PubMed: 26630549]

(53). Keinanen O, Li XG, Chenna NK, Lumen D, Ott J, Molthoff CF, Sarparanta M, Helariutta K, Vuorinen T, Windhorst AD et al. (2016) A new highly reactive and low lipophilicity fluorine-18 labeled tetrazine derivative for pretargeted PET imaging. ACS Med. Chem. Lett 7, 62–66. [PubMed: 26819667]

(54). Guo J, Lang L, Hu S, Guo N, Zhu L, Sun Z, Ma Y, Kiesewetter DO, Niu G, Xie Q et al. (2014) Comparison of three dimeric ^{18}F-AlF-NOTA-RGD tracers. Mol. Imaging Biol. 16, 274–83. [PubMed: 23982795]

(55). Lemaire M, D'Huyvetter M, Lahoutte T, Van Valckenborgh E, Menu E, De Bruyne E, Kronenberger P, Wernery U, Muyldermans S, Devoogdt N et al. (2014) Imaging and radioimmunotherapy of multiple myeloma with anti-idiotypic nanobodies. Leukemia 28, 444–47. [PubMed: 24166214]

(56). Lindmo T, Boven E, Cuttitta F, Fedorko J, and Bunn PA Jr. (1984) Determination of the immunoreactive fraction of radiolabeled monoclonal antibodies by linear extrapolation to binding at infinite antigen excess. J. Immunol. Methods 72, 77–89. [PubMed: 6086763]

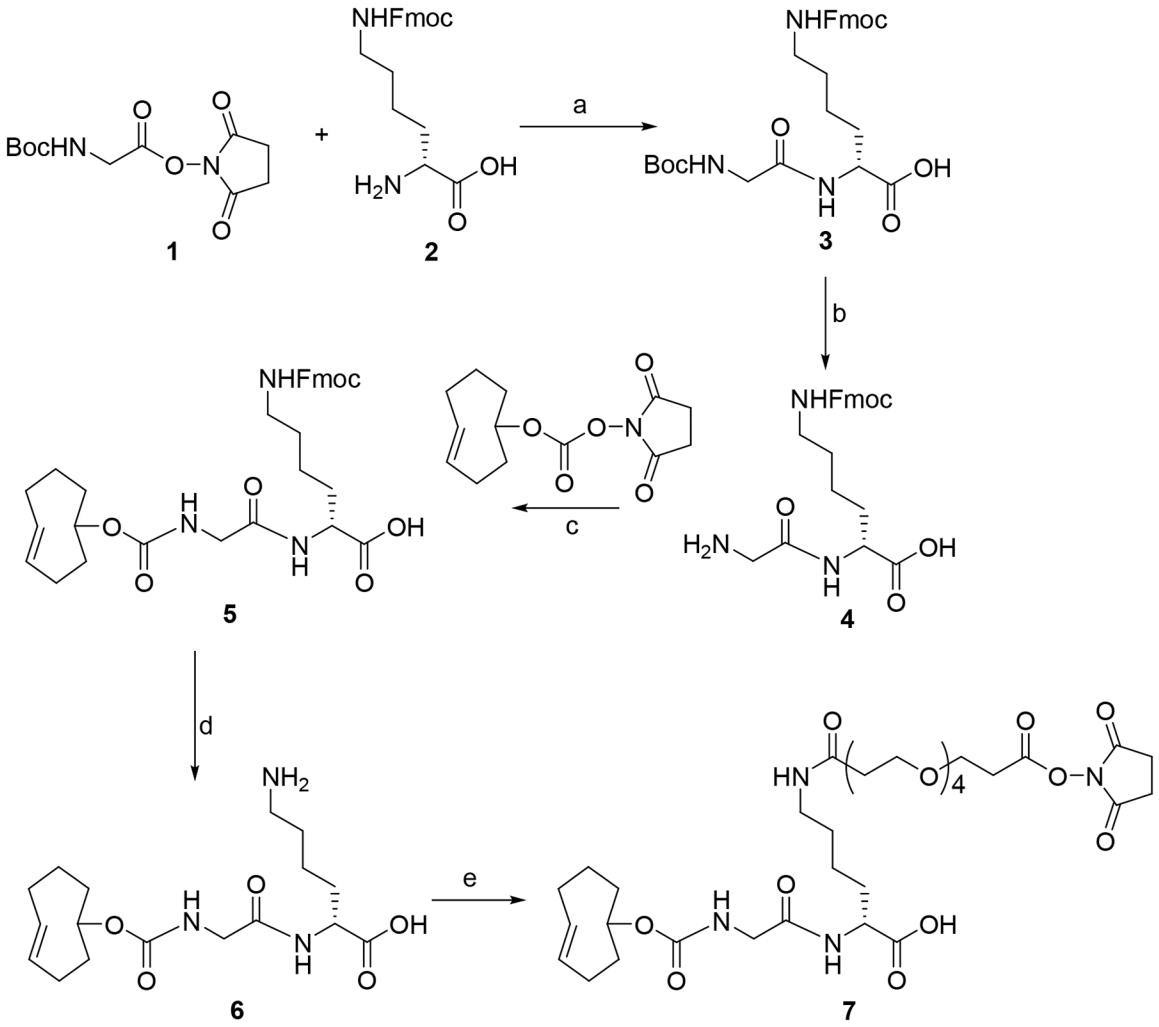

Scheme 1.

Scheme forthe synthesis ofTCO-GK-PEG$_4$-NHS ester.

a) DIEA, DMF b) 95:2.5:2.5 TFA:water:triisopropylsilane c) TCO-NHS, DIEA, DMF d) 20% Piperidine in DMF e) NHS-PEG$_4$-NHS, DIEA

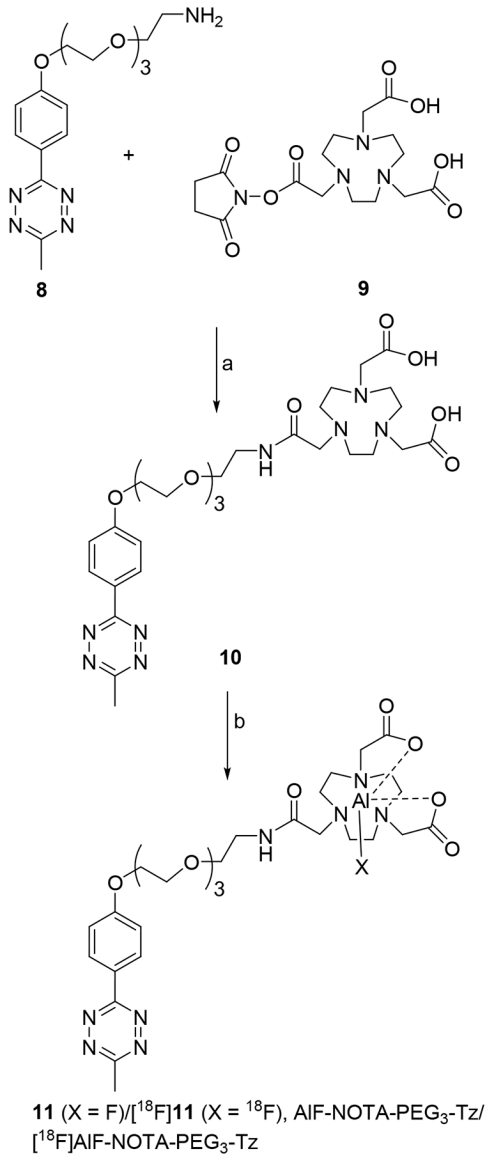

Scheme 2.

Scheme forthe synthesis ofAlF-NOTA-PEG_3-Tz and [^{18}F]AlF-NOTA-PEG_3-Tz.

a) DIEA, DMF b) AlF_3 or [^{18}F]fluoride and $AlCl_3$, acetate buffer, pH 4, acetonitrile

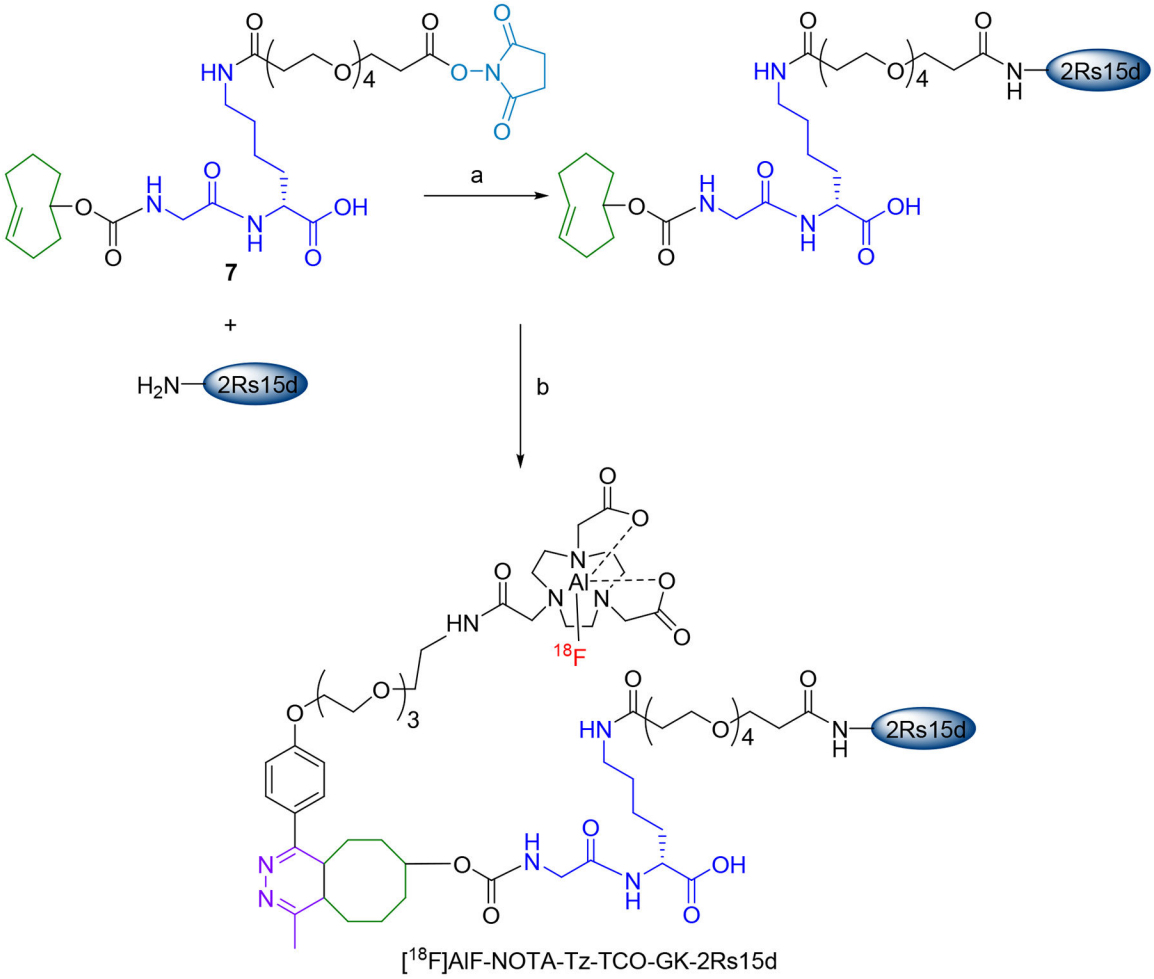

Scheme 3.

Pre-derivatization of 2Rs15d with 7 and subsequent ^{18}F-labeling via IEDDAR with 11. a) Borate buffer, pH 8.5, 30°C, 2 h b) [^{18}F]11, PBS, pH 7.4, 20°C, 10 min.

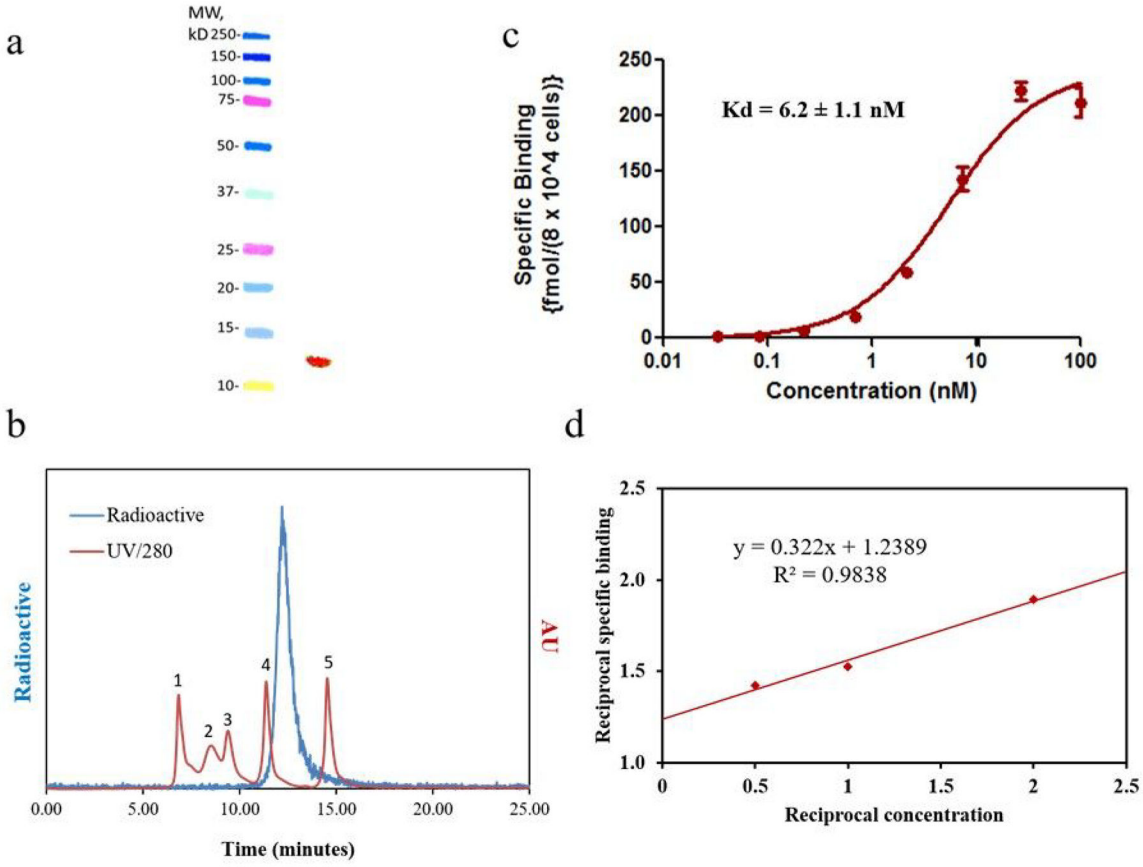

Figure 1.

In vitro quality control data for [^{18}F]AlF-NOTA-Tz-TCO-GK-2Rs15d. **a**) SDS-PAGE/ phosphor imaging (right lane) shows only one band corresponding to the molecular weight of 2Rs15d sdAb; molecular weight markers are shown in the left lane, **b**) Size-exclusion HPLC profile of the labeled 2Rs15d (blue line). As a reference, the UV HPLC profile of standards of different molecular weight is also shown (red line)—1) thyroglobulin (670 kDa), 2) γ-globulin (158 kDa), 3) ovalbumin (44 kDa), 4) myoglobin (17 kDa), 5) vitamin B12 (1.4 kDa). c) Saturation binding assay performed on HER2-positive SKOV-3 cells (mean ± SD). d) Immunoreactivity assay to determine binding to HER2 ECD at infinite antigen excess.

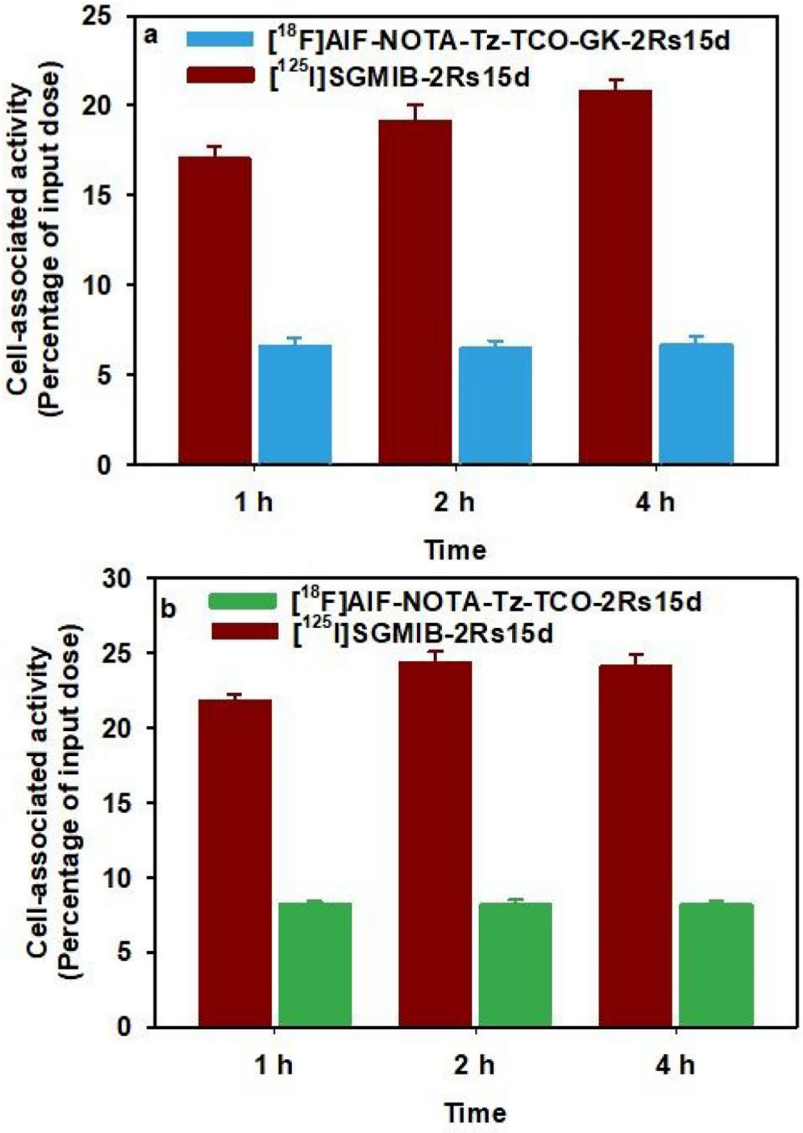

Figure 2.

Paired-Iabel uptake of [^{125}I]SGMIB-2Rs15d and **a**) [^{18}F]AIF-NOTA-Tz-TCO-GK-2Rs15d or b) [^{18}F]AIF-NOTA-Tz-TCO-2Rs15d. SKOV-3 cells were Incubated with [^{125}I]SGMIB-2Rs15d (dark red) and [^{18}F]AIF-NOTA-Tz-TCO-GK-2Rs15d (cyan) or [^{18}F]AIF-NOTA-Tz-TCO-2Rs15d (green) at 37°C and processed at 1, 2 and 4 h as described in the text. Data (mean ± SD) shown are percent of initially added activity that remained specifically (total minus nonspecific) bound to cells.

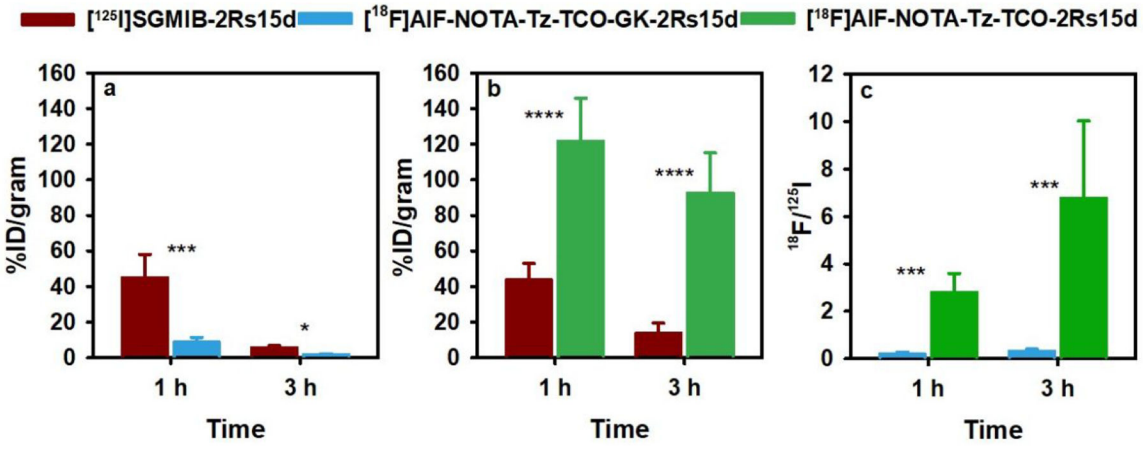

Figure 3.

Paired-Iabel kidney uptake of [^{125}I]SGMIB-2Rsl5d (dark red) and a) [^{18}F]AIF-NOTA-Tz-TCO-GK-2Rs15d (cyan) and b) [^{18}F]AIF-NOTA-Tz-TCO-2Rs15d (green) in normal mice c) Uptake of ^{18}F-Iabeled compounds, normalized to co-administered [^{125}I]SGMIB-2Rs15d in each study (^{18}F/^{125}I) are presented.

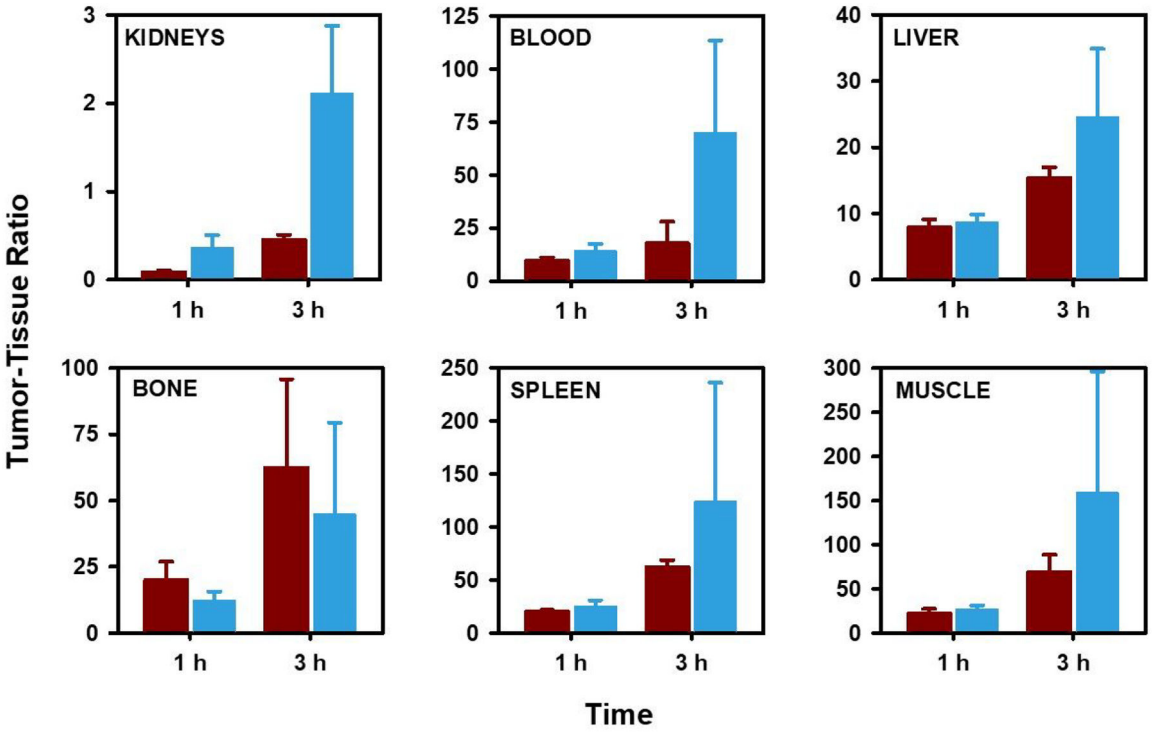

Figure 4.

Tumor-to-tissue ratios at 1 h and 3 h obtained from the paired-label biodistribution of [^{125}I]SGMIB-2Rs15d (dark red) and [^{18}F]AIF-NOTA-Tz-TCO-GK-2Rs15d (cyan) in athymic mice bearing SKOV-3 human ovarian cancer xenografts.

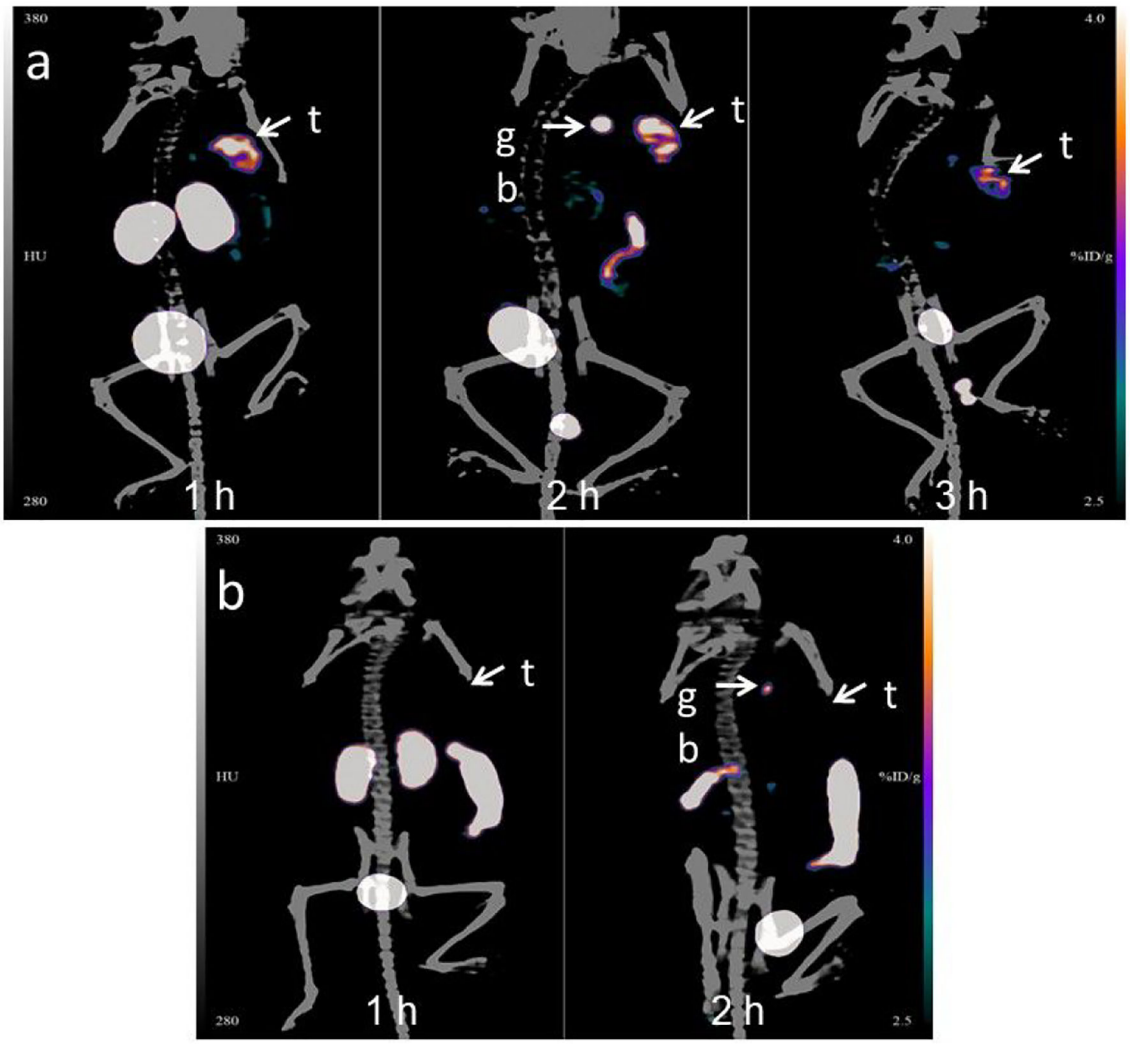

Figure 5.

a) Maximum intensity projection images obtained by the microPET/CT imaging of a representative mouse bearing SKOV-3 human ovarian cancer xenograft 1 h, 2 h and 3 h after administration of [^{18}F]AIF-NOTA-Tz-TCO-GK-2Rs15d, B) Images obtained at 1 h and 2 h after administration of [^{18}F]AIF-NOTA-Tz-TCO-GK-R3B23 control sdAb. Positions of tumor (t) and gall bladder (gb) are indicated.

Table 1.

Comparison of synthetic methods for labeling the sdAb 2Rs15d with ^{18}F.

Parameters	[^{18}F]RL-I-2Rs15d (Ref.37)	[^{18}F]RL-II-2Rs15d (Ref.22)	[^{18}F]AlF-NOTA-Tz-TCO-GK- 2Rs15d
Total time for synthesis	3.0 h	2.0 h	1.5 h
Heating cycles	3	1	1
Total time for heating	50 min	15 min	15 min
Evaporation cycles	6	4	1
HPLC required	Yes, Normal phase	Yes, Reversed-phase	No
Extraction required	Yes	No	No
Cartridge other than QMA	Na_2SO_4	C18 SPE	C18 SPE
TFA cleavage required	Yes	No	No
RCY for intermediate	8.5 ± 2.8%	55.9 ± 14.5%	46.3 ± 4.1%
Conjugation yield	40.8 ± 9.1%	23.9 ± 6.9%	52.0 ± 1.8%
Overall RCY	3.5 ± 1.0%	3.2 ± 0.9% (n = 8)	17.8 ± 1.5% (n = 5)

Table 2.

Paired-label biodistribution of [^{18}F]AlF-NOTA-Tz-TCO-GK-2Rs15d and [^{125}I]SGMIB-2Rs15d in athymic mice bearing subcutaneous SKOV-3 ovarian cancer xenografts.

Tissues	Percent injected dose per gram[a]			
	1 h		3 h	
	I-125	F-18	I-125	F-18
Liver	0.55 ± 0.05	0.40 ± 0.05	0.25 ± 0.05	0.13 ± 0.07
Spleen	0.28 ± 0.02	0.14 ± 0.02	0.13 ± 0.04	0.03 ± 0.02
Lungs	0.66 ± 0.03	0.43 ± 0.05	0.22 ± 0.05	0.16 ± 0.03[c]
Heart	0.29 ± 0.01	0.14 ± 0.02	0.11 ± 0.04	0.02 ± 0.02
Kidneys	52.36 ± 11.55	10.48 ± 3.91	8.50 ± 0.72	1.50 ± 0.66
Stomach	1.28 ± 0.40	0.35 ± 0.21	0.98 ± 0.54	0.04 ± 0.02
Sm. Int.	0.53 ± 0.11	1.99 ± 0.46	0.15 ± 0.04	0.24 ± 0.11[c]
Lg. Int.	0.18 ± 0.04	0.14 ± 0.09[c]	0.40 ± 0.15	2.81 ± 0.60
Thyroid[b]	0.80 ± 0.18	0.03 ± 0.04	0.88 ± 0.46	0.01 ± 0.02
Muscle	0.21 ± 0.05	0.13 ± 0.02	0.06 ± 0.03	0.01 ± 0.03
Blood	0.46 ± 0.04	0.25 ± 0.03	0.30 ± 0.20	0.05 ± 0.03
Bone	0.23 ± 0.08	0.29 ± 0.07[c]	0.08 ± 0.04	0.10 ± 0.07[c]
Brain	0.04 ± 0.02	0.02 ± 0.01[c]	0.01 ± 0.00	0.00 ± 0.01[c]
Tumor	4.31 ± 0.52	3.46 ± 0.40	3.82 ± 0.65	2.80 ± 0.31

[a]Mean ± SD (n = 5);

[b]Percent injected dose per organ;

[c]Difference in the uptake between the two agents statistically not significant.